From carbonate-sulphate interbeds to carbonate breccias: the role of tectonic deformation and diagenetic processes (Cameros Basin, Lower Cretaceous, N Spain)

I. Emma Quijada[a,b*], Pablo Suarez-Gonzalez[a,b], M. Isabel Benito[a,b], Stefano Lugli[c], Ramón Mas[a,b]

[a] *Departamento de Estratigrafía, Universidad Complutense de Madrid, C/ José Antonio Novais 12, 28040 Madrid, Spain*

[b] *Instituto de Geociencias IGEO (CSIC, UCM), C/ José Antonio Novais 12, 28040 Madrid, Spain*

[c] *Dipartimento di Scienze Chimiche e Geologiche, Università degli Studi di Modena e Reggio Emilia, largo Sant'Eufemia 19, 41121 Modena, Italy*

* Corresponding author: Tel.: +34913944783. Fax: +34913944808. E-mail address: equijada@geo.ucm.es

ABSTRACT

Interpreting the origin of carbonate breccias requires a detailed analysis because they may be the result of a wide variety of processes that produce similar features. This is the case of the Lower Cretaceous carbonate breccias of the Cameros Basin (previously interpreted as slump or collapse breccias), whose origin is interpreted after performing a detailed sedimentary, petrographic and tectonic study.

The studied carbonate breccias consist of angular carbonate mudstone fragments floating in a matrix of calcite and quartz crystals. The breccias are interbedded with, and laterally associated to, alternating layers of carbonate mudstone and calcite and quartz pseudomorphs after gypsum, which show strong similiarities to the breccia fragments and matrix, respectively, suggesting that the brecciated beds were originally composed of identical alternating carbonate mudstone and gypsum layers as the unbrecciated layers. The breccias are associated with frequently polyharmonic

deformation structures, which are similarly oriented as the regional tectonic structures, indicating that they are related with the alpine contractional deformation of this area of the Cameros Basin.

All these features suggest that the carbonate breccias were formed by tectonic deformation of alternating layers of carbonate mudstone and calcium sulphate, which have very different rheological behaviour. As a result, during tectonic deformation, sulphate flowed and carbonate layers were broken and displaced, producing a breccia of carbonate fragments within a sulphate groundmass. Afterwards, the sulphate groundmass was replaced by quartz and calcite, and the breccia acquired its final composition.

Keywords: Carbonate brecciation, carbonate-sulphate deposits, tectonic deformation, tectonically-driven evaporite flow, Lower Cretaceous, Cameros Basin.

1. Introduction

Carbonate breccias are sedimentary rocks made up of gravel-sized, angular, limestone or dolostone fragments embedded in a groundmass consisting of fine-grained matrix and/or cements (Flügel, 2010, and references therein). Carbonate breccias may be formed by a wide variety of syn- and post-depositional processes (e.g. Norton, 1917; Blount and Moore, 1969; Richter and Füchtbauer, 1981; Flügel, 2010), such as

deposition of eroded material, pedogenesis, slumps, faulting, or collapse caused by solution of evaporites or carbonates. For this reason, an appropriate interpretation of the process that caused the carbonate breccias may be an essential clue to understand either the sedimentary environment or the diagenetic or tectonic processes. However, classifying these rocks is often challenging because different processes may produce similar features, and thus, lead to completely different interpretations about the sedimentary environment or the post-depositional processes (e.g. Norton, 1917; Blount and Moore, 1969; Hoffman et al., 2009; Flügel, 2010, and references therein; Vlahovic et al., 2012).

The carbonate breccias of the Lower Cretaceous Oncala Group from the Cameros Basin (northern Spain) show several features that could lead to interpret them as the result of slumps (Salomon, 1982; Gómez-Fernández, 1992; Gómez-Fernández and Meléndez, 1994a; Meléndez and Gómez-Fernández, 2000), and some other characteristics suggest that they could be related with evaporite-solution collapse (Gómez-Fernández, 1992; Gómez-Fernández and Meléndez, 1994a; Meléndez and Gómez-Fernández, 2000; Mas et al., 2002). However, the integrated analysis of field and petrographic data suggests a new brecciation mechanism related with tectonic, frequently polyharmonic, deformation of two interbedded lithologies (carbonates and sulphates) with different rheological behaviours. Although tectonically-driven evaporite-flow processes have been described in the literature from décollement horizons of thrust faults (Helman and Schreiber, 1985; Lugli, 2001; Schreiber and Helman, 2005; Warren, 2006), to our knowledge, the formation of tectonic sulphate-flow carbonate breccias unrelated to thrusts has not been studied. This is the case of the carbonate breccias of the Oncala Group, which were developed in an area deformed by large-scale folds. The studied deposits provide an excellent example to understand this

brecciation mechanism, because all the different stages of deformation, from undisturbed strata to slightly deformed and chaotic beds, can be observed. Moreover, it is possible to compare the calcitized sulphate-carbonate deposits present in most of the Oncala Group with uncalcitized gypsum-carbonate deposits preserved in a small area of the basin, which allows us to verify the proposed tectonic sulphate-flow brecciation model. The aim of the present study is to interpret the brecciation mechanism that caused the carbonate breccias of the Oncala Group by combining all the sedimentary, petrographic and tectonic criteria available. Furthermore, this article provides criteria to recognize similar breccias in other ancient successions, which may be useful for avoiding confusion with synsedimentary slump breccias caused by gravity instability, or with diagenetic collapse breccias formed after dissolution of sulphates by meteoric waters undersaturated in $CaSO_4$. The recognition of tectonic sulphate-flow breccias may also be useful to identify intense structural deformation in, otherwise, apparently undeformed successions.

2. Geological setting

The studied carbonate breccias are part of the sedimentary infill of the Cameros Basin, northern Spain (Fig. 1A), which is the northwesternmost basin of the Mesozoic Iberian Rift System (Mas et al. 1993; Guimerà et al., 1995). The Cameros Basin was formed during Late Jurassic to Early Cretaceous intraplate rifting in Iberia as a consequence of the opening of the North Atlantic Ocean (Álvaro et al., 1979; Vegas and Banda, 1982; Salas et al., 2001). This basin recorded high subsidence and accumulation rates, with more than 6000 m of vertical thickness of sediments from the Tithonian to the early Albian (Mas et al., 2011; Omodeo-Salè et al., 2014). The infill of the Cameros

Basin corresponds to a large cycle or supersequence divided into eight depositional sequences (Fig. 1B), which consist of continental and coastal deposits (Mas et al., 1993; 2011; Quijada et al., 2013b, in press; Suarez-Gonzalez et al., 2013, 2014, in press). The Cameros Basin was affected by two hydrothermal metamorphic events during the mid-Cretaceous and the Eocene, which reached temperatures up to 350-410ºC and 300ºC, respectively (e.g. Alonso-Azcárate et al., 1995, 1999; Mata et al., 2001; Mantilla-Figueroa et al., 2002; González-Acebrón et al., 2011). The Cameros Basin was uplifted from the Paleogene to the middle Miocene due to the Alpine Orogeny (Casas-Sainz and Simón-Gómez, 1992; Mas et al., 1993; Guimerà et al., 1995).

The Oncala Group, which contains the studied carbonate breccias, corresponds to the third depositional sequence of the basin (Mas et al., 1993, 2002; Gómez-Fernández and Meléndez, 1994b), and was deposited in the eastern sector of the Cameros Basin (Fig. 1A) during the Berriasian (Salomon, 1982; Schudack and Schudack, 2009). The Oncala Group contains both siliciclastic and carbonate-evaporitic deposits, which are laterally related (Fig. 1). Western to central areas of the Oncala Group consist of siliciclastic deposits interpreted as formed in fluvial systems in westernmost areas (Gómez-Fernández and Meléndez, 1994a,1994b; Meléndez and Gómez-Fernández, 2000; Quijada et al., 2013b) and broad tidal flats in central areas (Quijada et al., 2013b, in press). The tidal siliciclastic deposits change gradually eastwards to carbonate-evaporitic deposits, which are interpreted as formed in coastal, shallow, carbonate-sulphate water bodies and their mudflats (Quijada et al., 2013a, 2013b). The carbonate-evaporitic deposits consist mainly of alternating laminae of carbonate mudstone and calcite and quartz pseudomorphs after gypsum, and show a progressive increase in the proportion of evaporitic deposits relative to carbonates from the central to the eastern areas of the basin, in that the evaporitic laminae become thicker and more abundant.

126 The alternating carbonate-evaporitic deposits are interbedded with carbonate breccias in
127 the eastern area of the basin (Fig. 2). The carbonate-evaporitic deposits of the eastern
128 area of the Oncala Group have been subdivided in two different formations (Figs. 2, 3):
129 the lower Aguilar del Río Alhama Formation and the upper Valdeprado Formation
130 (sensu Quijada et al., 2013b), the former containing larger amounts of evaporitic
131 deposits and carbonate breccias. The Oncala Group is one of the thickest units of the
132 Cameros Basin comprising up to 2500 m of sediments in the depocentral area of the
133 basin, which is located within the studied area and consists mainly of carbonate-
134 evaporitic deposits (stratigraphic section of Aguilar, Figs. 2, 3).
135 The carbonate-evaporitic deposits were probably buried under more than 5500 m of
136 Cretaceous sediments (Omodeo-Salè et al., 2014), according to measurements in cross-
137 sections of adjacent areas, and reached temperatures of at least ≈225ºC (Alonso-
138 Azcárate et al., 2001, 2006), based on analysis of the carbonate-evaporitic deposits of
139 the easternmost area of the Oncala Group, or even of more than 350-410ºC (Mata et al.,
140 2001; González-Acebrón et al., 2011, 2012), considering data from the underlying Tera
141 Group (Fig. 1B). Moreover, the eastern area of the Cameros Basin, where the carbonate
142 breccias occur, is deformed by regional, NW-SE trending folds (Fig. 2; Gil-Imaz et al.,
143 1990; Gil-Imaz and Pocoví, 1991, 1994). These structures deform the Oncala Group
144 (especially the lower carbonate-evaporitic deposits, i.e. the Aguilar del Río Alhama
145 Formation, Figs. 2, 3) and the underlying rocks, but most of them do not deform the
146 overlying deposits (Fig. 2). It has been interpreted that these tectonic structures were
147 developed during the Alpine Orogeny by reactivation of fracture zones that controlled
148 sedimentation of the Oncala Group (Gómez-Fernández, 1992; Gómez-Fernández and
149 Meléndez, 1994b; Quijada et al., 2013b).
150

3. Methodology

Geological mapping of the Oncala Group was performed using field observations, aerial photographs, and satellite images (Fig. 2). Two selected stratigraphic sections (Aguilar and Cervera sections) were logged in detail from base to top of the Oncala Group in the eastern area of the basin (Figs. 2, 3). Numerous additional individual outcrops of the carbonate breccias have been studied in order to collect data on their geometry, structures, relationships to adjacent rocks, and composition.

Structural analysis (Fig. 2) was performed in order to establish the relationship between the regional tectonic structures and the folds observed in the deposits of the Oncala Group. 27 strike and dip measurements of bedding were taken along the Pégado anticline, and 11 measurements along the Inestrillas syncline. Measurements were analyzed using Stereonet 8 software, based on OSXStereonet by Cardozo and Allmendinger (2013), in order to calculate the attitude of the axial planes of these regional folds. The axial planes of 99 decimetre to metre-scale folds, measured in six different outcrops of the Oncala Group, were represented on stereographic projections using OpenStereo software (Grohmann and Campanha, 2010).

A total of 289 rock samples were collected for petrographic analysis under transmitted light microscopy. Half of each thin section was stained with Alizarin Red S and potassium ferricyanide (Dickson, 1966). Limestones and dolostones were classified according to Dunham's (1962) classification, and gypsum was classified according to the classification by Ciarapica et al. (1985).

Selected samples were analysed with JEOL JSM 6400 scanning electron microscope at the Laboratory of Geological Techniques of the Complutense University of Madrid.

4. Sedimentary facies associated with the carbonate breccias

The carbonate breccias of the Oncala Group occur in the eastern area of the Cameros Basin, in the area located eastwards of the town of Valdemadera (Fig. 2). The most abundant sedimentary facies in this area is an alternation of layers of carbonate mudstone and calcite and quartz pseudomorphs after gypsum (Quijada et al., 2013a, 2013b), which is interbedded with the carbonate breccias (Figs. 3, 4). Siliciclastic mudstone layers composed of clay, very-fine-silt-size quartz and mica grains, iron oxides, and variable carbonate contents are also present in the succession (Figs. 3, 4).

The carbonate mudstone-pseudomorphs after gypsum alternation is made up of laterally continuous and parallel layers, which can be followed tens or even hundreds of metres (Fig. 5A). Carbonate mudstone layers are generally submillimetre to 10 cm in thickness, and they consist mainly of calcitic or dolomitic mudstone (Figs. 5B, C) with up to 20% of silt-size grains of quartz, calcite, and mica. Carbonate mudstone layers commonly contain disperse calcite and quartz pseudomorphs after (sub-) millimetre-size lenticular gypsum (Quijada et al., 2013a, Fig. 5C).

Layers of calcite and quartz pseudomorphs are submillimetre to 5 cm in thickness (Figs. 5B, C), and they are composed of a mosaic of cloudy pseudosparitic calcite with micrite, anhydrite and quartz inclusions, and minor cloudy macrocrystalline quartz with abundant anhydrite inclusions (Figs. 5C-F, 6). The calcite and quartz crystals are arranged in aggregates of pseudomorphs after crystals displaying generally lenticular habit (Figs. 5C-F), and the carbonate mudstone matrix around them is deformed.

The proportion of pseudomorphs after gypsum compared to carbonate mudstone in the Oncala Group increases gradually northeastwards because the layers of pseudomorphs after gypsum become progressively thicker and more abundant.

Moreover, layers of calcite and quartz pseudomorphs after gypsum are also more abundant and thicker in the lower part of the succession, i.e. the Aguilar del Río Alhama Formation, than in the upper part, i.e. the Valdeprado Formation (Figs. 3, 4).

The carbonate breccias (described below in detail) and the facies associated with them are commonly arranged in 50 cm to 10 m-thick sequences (Fig. 7A). The lower part of the sequences consists commonly of siliciclastic mudstones, and progressively changes to alternating layers of carbonate mudstone and calcite and quartz pseudomorphs after gypsum, which show a gradual increase upwards in the proportion of pseudomorphs after gypsum beds compared to carbonate mudstone beds. Carbonate breccias are commonly present at the top of these sequences (Fig. 7).

The alternating layers of carbonate mudstone and calcite and quartz pseudomorphs after gypsum of the Oncala Group have been interpreted as deposited in shallow, perennial, carbonate-sulphate, coastal water bodies, developed in a flat-bottomed basin (Quijada et al., 2013a, 2013b). Sedimentation in these water bodies was strongly controlled by alternation of flooding and evaporative intervals, which caused salinity fluctuations (Quijada et al., 2013a). As a consequence, carbonate mudstone was deposited during lower-salinity periods following water discharge, and gypsum precipitated during higher-salinity periods caused by progressive evaporation. The lenticular habits that show generally the pseudomorphs after gypsum (Figs. 5C-E) and the deformation of the carbonate matrix around them, suggest that most of the gypsum precipitated displacively within the carbonate mud, in the upper part of the sedimentary column, or at the sediment-water interface (cf. Magee, 1991; Kendall, 1992; Ortí, 2010a). The larger proportion of pseudomorphs after gypsum compared to carbonate mudstone in the northeastern areas of the basin was probably related with higher salinities caused by a lower freshwater input in these areas (Quijada et al., 2013b). The

lower proportion of evaporites in the upper part of the Oncala Group, i.e. the Valdeprado Formation, than in the lower part, i.e. the Aguilar del Río Alhama Formation (Figs. 2, 3), was probably due to shorter periods of confined conditions in the carbonate-sulphate water bodies, which caused predominance of lower salinities (Quijada *et al.*, 2013b).

5. Carbonate breccias

Carbonate breccias of the Oncala Group occur in the eastern area of the Cameros Basin, and they are interbedded with, and pass laterally to, alternating layers of carbonate mudstone and calcite and quartz pseudomorphs after gypsum (Figs. 8, 9). The carbonate breccia layers range from few centimetres to up to 12 m in thickness, and they can be laterally followed for hundreds of metres (Fig. 4). Carbonate breccias are especially abundant and thicker in the lower part of the Oncala Group (i.e. Aguilar del Río Alhama Formation; Figs. 2, 3), which is characterized by intense deformation, and are thinner and less common in the less deformed upper part (i.e. Valdeprado Formation; Figs. 2, 3, 4B). Moreover, the carbonate breccia beds thicken and are more abundant northeastwards (Figs. 2, 4B). The contacts of the breccias with the underlying and the overlying layers of alternating carbonate mudstone and pseudomorphs after gypsum are generally irregular (Figs. 8A, 8B, 9A), but may show sharp lower and upper limits (Figs. 8D, 9B).

The carbonate breccias of the Oncala Group are made up of fragments of carbonate mudstone floating in a matrix composed of calcite and quartz crystals (Figs. 8, 9, 10, 11). The fragments of carbonate mudstone have rectangular prismatic shape, and they range from few millimetres to 10 cm in size. Carbonate mudstone fragments commonly

include disperse calcite and quartz pseudomorphs after gypsum (Fig. 11A), and they may contain up to 20% of silt-size grains of quartz, calcite, and mica. The matrix around the fragments consists mainly of a mosaic of cloudy pseudosparitic calcite with micrite, anhydrite and quartz inclusions, and less abundant macrocrystalline quartz with abundant anhydrite inclusions (Fig. 11).

The carbonate breccias of the Oncala Group are generally matrix-supported, and the fragments may be from very slightly displaced (Figs. 10A, 10B) to chaotically arranged (Figs. 7B, 8, 10C). The orientation of the fragments commonly allows the recognition of the original mudstone bedding and the identification of folds (Figs. 9, 10). The most intense brecciation and displacement of the fragments occurs generally in the core of the folds, where breccias commonly display chaotic fabrics (Figs. 8B, 8C, 10B, 10C).

6. Carbonate-gypsum layers of the easternmost area of the basin

The lower part of the Oncala Group in the easternmost area of the basin (Fig. 2) is characterized by an alternation of layers of dolomudstone and gypsum (Figs. 3, 12). These deposits consist of submillimetre to 10 cm-thick, laterally continuous, parallel layers, which can be followed for hundreds of metres. Dolomudstone layers commonly include disperse gypsum crystals (Fig. 12B), and may contain up to 20% of silt-size grains of quartz and mica. Gypsum layers consist mainly of xenotopic granular gypsum (Figs. 12C, D, F), but macrocrystalline and xenotopic, irregular, cloudy crystals occur in some layers (Fig. 12E). Macrocrystalline gypsum contains inclusions of anhydrite (Fig. 12E). Some gypsum layers include a few macrocrystalline quartz crystals with anhydrite inclusions (Fig. 12F).

7. Deformational features

Deposits of the eastern area of the Oncala Group show important deformational features, which affect both the carbonate mudstone-pseudomorphs after gypsum alternation and the carbonate breccias (Figs. 8B, 8C, 9, 10, 11, 13, 14, 15A-D). In fact, the presence of carbonate breccias is intimately related to these deformational structures (Figs. 8B, 8C). Moreover, the alternating carbonate-gypsum layers of the easternmost area of the basin are also deformed (Figs. 15E-G), which causes disruption of the dolomudstone layers into rectangular fragments that float in a gypsum groundmass (Figs. 12C, 12D, 15F).

In the lower part of the Oncala Group, i.e. the Aguilar del Río Alhama Formation (Figs. 2, 3), the deformational features consist of polyharmonic folding made up of folds of large wavelengths and amplitudes that contain parasitic folds of smaller wavelengths and amplitudes (Figs. 9A, 13, 14, 15A-D). That is, larger-scale folds that show amplitudes of tens of metres contain folds with amplitudes of decimetres to metres, which in turn include smaller folds with amplitudes of millimetres to centimetres. Apart from polyharmonic folds affecting multi-layered sequences, interstratal folds occur also in some beds (Fig. 8D, 9B, 15G).

The most abundant axial planes of the measured decimetre to metre-scale folds strike about NW-SE (between N114ºE and N168ºE, maximum density at N140ºE) in five out of six measurement sites (Fig. 2; Supplementary Data Table 1), although the axial planes of the folds in the northeasternmost site strike between N140ºE and N220ºE, maximum density at N167.1ºE (Fig. 2; Supplementary Data Table 1). Most of these folds are upright folds (axial planes dip between 80º and 90º) or steeply inclined folds (dips between 60º and 79º), although the axial planes of 28 folds dip less than 60º

(Fig. 2; Supplementary Data Table 1). These predominantly NW-SE orientations of the folds are consistent with the regional major structures in the area, whose attitude has been calculated based on strike and dip measurements of the bedding (Fig. 2; Supplementary Data Tables 2 and 3). The calculated attitude of the axial plane of the Pégado anticline is N144ºE/82ºW, and that of the Inestrillas syncline is N155ºE/80ºNE (Fig. 2).

The upper part of the Oncala Group, i.e. the Valdeprado Formation (Figs. 2, 3), which is not affected by such intense regional deformation, does not present polyharmonic folds, but shows occasional folds with amplitudes of centimetres to decimetres. The carbonate breccias in the upper part of the succession are generally related with these deformational structures (Fig. 8B).

8. Discussion

8.1. Origin of breccia fragments and matrix

An essential part of the interpretation of carbonate breccias is the compositional analysis of the fragments and matrix to determine source, depositional or post-depositional formation, and relative timing of formation (e.g. Richter and Füchtbauer, 1981; Dozet, 1996; Flügel, 2010, and references therein). To achieve this, it is essential to compare the fragments and matrix of the breccias with the associated unbrecciated deposits. Carbonate breccias of the Oncala Group are interbedded with, and pass laterally to, alternating layers of carbonate mudstone and calcite and quartz pseudomorphs after gypsum (Quijada et al., 2013a, 2013b, Figs. 5, 7B, 8A). The breccia fragments display very similar features to the unbrecciated carbonate mudstone layers

(Figs. 7B, 8, 9, 10, 11), and also contain disperse calcite and quartz pseudomorphs after gypsum and up to 20% of clastic grains. These characteristics suggest that the carbonate breccias are made up of intraformational fragments derived from the breaking apart of the carbonate mudstone layers that constitute the Oncala Group in the eastern area of the Cameros Basin.

The unbrecciated layers of calcite and quartz pseudomorphs after gypsum are characterized by a mosaic of cloudy pseudosparitic calcite with micrite, anhydrite and quartz inclusions, and less abundant cloudy macrocrystalline quartz with abundant anhydrite inclusions (Figs. 5C-F, 6), which is the same composition as the matrix of the carbonate breccias of the Oncala Group (Fig. 11). These resemblances suggest that the mosaics of calcite and quartz of both the unbrecciated and brecciated layers had the same origin, that is, they originally were gypsum layers. This statement is confirmed by the preservation of uncalcitized deposits in the lower part of the succession at the easternmost area of the Oncala Group (Figs. 2, 3, 12, 15E-G), which consist of an alternation of carbonate and gypsum layers that display identical features to the calcitized deposits (Figs. 8-11).

The Oncala Group deposits were progressively buried more than 5500 m (Omodeo-Salè et al., 2014) reaching temperatures of at least ≈225ºC (Alonso-Azcárate et al., 2001, 2006). As gypsum is not stable at burial conditions (e.g. Macdonald, 1953; Jauzein, 1974; Shearman, 1983; Jowett et al., 1993), gypsum deposits of the Oncala Group were dehydrated to anhydrite. Nevertheless, anhydrite becomes unstable during uplift due to meteoric flushing and/or surface weathering, which results in its hydration and conversion into secondary gypsum (Holliday, 1970; Lugli, 2001; Warren, 2006). This process also occurred in the Oncala Group during Alpine uplifting of the area and during weathering, causing anhydrite conversion into secondary gypsum, still preserved

in the easternmost areas of the basin (Figs. 2, 3, 12, 15E-G). The xenotopic granular, macrocystalline and xenotopic irregular cloudy gypsum textures (Figs. 12C-E) and the anhydrite relicts within the gypsum (Fig. 12E) strongly support this interpretation (cf. Holliday, 1970; Ciarapica et al., 1985; Lugli, 2001). However, the presence of cloudy pseudosparitic calcite with anhydrite inclusions in most of the Oncala Group (Figs. 3, 5, 6, 11) suggests that most of the sulphate of the succession (except that of the easternmost area) was calcitized during uplift, which is a process widely documented from meteoric settings via flushing of groundwaters undersaturated with respect to $CaSO_4$ and supersaturated with respect to $CaCO_3$ (e.g. Pierre and Rouchy, 1988; Warren, 2006).

Another question is the timing of quartz precipitation. The presence of quartz crystals with anhydrite inclusions within both the uncalcitized and calcitized rocks (Figs. 5E, 5F, 6, 11A, 11B, 11E, 12F) indicates that quartz precipitated during burial when sulphates were already transformed into anhydrite and prior to anhydrite hydration/calcitization. This interpretation is also supported by the presence of quartz inclusions within the pseudosparitic calcite and the corroded limits of the quartz crystals in contact with calcite (Fig. 6D).

8.2. Models for brecciation

8.2.1. Comparison with evaporite-solution collapse breccias

The evidence of vanished evaporites in the brecciated layers of the Oncala Group suggests that carbonate breccias may be the result of evaporite-solution collapse breccias (see Gómez-Fernández, 1992; Gómez-Fernández and Meléndez, 1994a; Meléndez and Gómez-Fernández, 2000; Mas et al., 2002). In this sense, the studied

breccias show some features typical of collapse breccias (Fig. 16), such as angular intraformational clasts and preservation of stratigraphic order of former intra-evaporite beds (McWhae, 1953; Middleton, 1961; Stanton, 1966; Beales and Oldershaw, 1969; Blount and Moore, 1969; Swennen et al., 1990; Papaioanou and Carotsieris, 1993; Eliassen and Talbot, 2005; Warren, 2006; Flügel, 2010). However, other features are not consistent with an evaporite-solution collapse origin (Fig. 16). Some of the most reliable characteristics of solution collapse breccias are sharp, planar, continuous lower contacts and gradational, irregular upper contacts that pass gradually to unaltered overlying deposits (Middleton, 1961; Beales and Oldershaw, 1969; Stanton, 1966; Eliassen and Talbot, 2005; Warren, 2006). On the contrary, the Oncala Group breccias show irregular upper and lower contacts (Figs. 8, 9A). Other significant features of the solution collapse breccias are the upward increase of clast support and decrease of clast translation degree (Middleton, 1961; Loucks et al., 2004; Eliassen and Talbot, 2005; Warren, 2006), which are not recognized in the studied carbonate breccias either. Moreover, the groundmass of solution collapse breccias normally consists of cements and/or a fine-grained matrix resulting from internal brecciation of coarser fragments (Middleton, 1961; Blount and Moore, 1969; Swennen et al., 1990; Papaioanou and Carotsieris, 1993; Eliassen and Talbot, 2005; Warren, 2006; Flügel, 2010), but the studied breccias contain evaporite-bearing matrix, which is rare in collapse breccias. Finally, evaporite-solution collapse processes cannot explain the deformation structures shown in the carbonate breccias of the Oncala Group (Figs. 8B, 8C, 9, 10, 11A, 11E, 15C, 15D). Although solution collapse of unconsolidated sediments may produce deformation structures, they would display irregular elongated conical zones of sinking in which the degree of deformation decreases upwards (Moretti et al., 2011), and disruption would be caused by vertical pressure. Moreover, if both brecciation and

401 deformation in the Oncala Group were caused by solution collapse processes,
402 deformation would occur exclusively in association with the brecciated layers, and
403 would not be present in the unbrecciated layers (Figs. 15A, 15B). Thus, a different
404 interpretation is necessary to explain the deformation structures observed in the
405 carbonate breccias of the Oncala Group, which seem to be closely related to the
406 brecciation origin.
407
408 *8.2.2. Comparison with slump breccias*
409 The intense deformation that occurs in the brecciated and unbrecciated carbonate-
410 evaporitic deposits of the Oncala Group share some similarities with the deformation
411 structures caused by slumps (Fig. 16), which led some authors to interpret them as the
412 result of this type of mass flow (Salomon, 1982; Gómez-Fernández, 1992; Gómez-
413 Fernández and Meléndez, 1994a; Meléndez and Gómez-Fernández, 2000). Slump beds
414 show significant internal distortion of the bedding, which includes folds, boudins,
415 (micro-) faults and internal shear surfaces, but the bedding is often still recognizable
416 (Martinsen, 1994; Stow et al., 1996; Posamentier and Martinsen, 2011; Tucker, 2011).
417 Moreover, slump deformation may show parasitic folds (Byrne, 1994), similar to those
418 of the described multilayered sequences with polyharmonic folds (Figs. 10, 13, 14,
419 15A-D). However, the deformed beds of the Oncala Group show numerous differences
420 with slumped layers indicating that they are not the result of mass-flow processes (Fig.
421 16). One of the differences is that slump folds are predominantly recumbent or
422 overturned folds (e.g. Woodcock, 1976; Spalluto et al., 2007; Tucker, 2011), whereas
423 upright or steeply inclined folds predominate in the Oncala Group (Fig. 2). Moreover,
424 slump folds are not geometrically related with regional tectonic folds (e.g. Woodcock,
425 1976), as occurs in the Oncala Group (Figs. 2, 14) suggesting that folding is related with

426 tectonic deformation instead of mass-flow processes. Furthermore, slump beds must
427 show evidence of synsedimentary origin, such as sharp lower and upper contacts with
428 the undisturbed layers below and above (Woodcock, 1976; Byrne, 1994; Cossey, 2011;
429 King et al., 2011; Tucker, 2011), erosional truncation of folds on the top surface
430 (Woodcock, 1976; Byrne, 1994; Stow et al., 1996; Cossey, 2011), or burrows,
431 dewatering structures and sand volcanoes at the top (Woodcock, 1976). On the contrary,
432 most of the deformed beds of the Oncala Group show irregular bases and tops (Figs.
433 8A-C, 9A), which do not truncate the structures, and evidence of synsedimentary origin
434 is absent. According to idealized models of slumps, the deformed units that result of
435 lateral mass movement of sediment show a well-defined upper extensional zone and a
436 downslope contractional zone (Martinsen, 1994; Posamentier and Martinsen, 2011),
437 which have not been recognized in the studied deposits. Furthermore, considering that
438 the sedimentary environment of the carbonate-evaporitic deposits of the Oncala Group
439 consisted in less than 10 m deep water bodies with very gentle slope gradients (Quijada
440 et al., 2013a, 2013b), it follows that hundreds of metre thick folded sequences as those
441 observed in the Oncala Group (Fig. 13B, 14) could not have been caused by gravity
442 instability. Finally, slump breccias are usually made up of clasts transported from
443 adjacent areas within a fine-grained sedimentary matrix, which commonly is brought
444 together with the clasts (e.g. Payros et al., 1999; Flügel, 2010, and references therein).
445 In contrast, the fragments and matrix of the studied carbonate breccias derive from in
446 situ brecciation of the carbonate-evaporitic deposits, as suggests the gradual lateral
447 change to unbrecciated layers of carbonate mudstone and calcite and quartz
448 pseudomorphs after gypsum (Figs. 8B, 9A). Moreover, slump breccias may show
449 primary sedimentary structures, such as normal or inverse grading (e.g. Peryt and

450 Kasprzyk, 1992; Payros et al., 1999; Flügel, 2010), which are absent in the Oncala
451 Group.
452
453 *8.2.3. Tectonic sulphate-flow breccia*
454 The evidence of a post-depositional origin for the deformation structures and their
455 strong geometrical relationships with the regional tectonic structures (similar NW-SE
456 trends; Figs. 2, 14) suggest that they formed during deformation related to the tectonic
457 uplift of the Cameros Basin during the Alpine Orogeny (see Casas-Sainz and Simón-
458 Gómez, 1992; Mas et al., 1993; Guimerà et al., 1995). As previously discussed, the
459 carbonate-evaporitic deposits of the Oncala Group were composed of alternating layers
460 of carbonate mudstone and anhydrite during burial, which have different rheological
461 behaviours. Experimental studies demonstrate that under differential stress fine-grained
462 anhydrite begins to flow readily at 150-180ºC, at strain rates of 10^{-14} s^{-1} (Müller and
463 Briegel, 1978; Müller et al., 1981; Schreiber and Helman, 2005), and field observations
464 suggest that anhydrite flow may begin at temperatures as low as 80ºC, at strain rates of
465 1.8-13×10^{-13} s^{-1} (Jordan and Nüesch, 1989). Limestone and dolostone beds, in contrast,
466 respond in a brittle manner at those temperatures. They start to deform by plastic flow at
467 temperatures above 350 ºC approximately, at strain rates of 10^{-12} s^{-1} (Müller and Briegel,
468 1978; Helman and Schreiber, 1985; De Bresser et al., 2002). Thus, considering that the
469 carbonate-sulphate deposits of the Oncala Group reached temperatures of at least
470 ≈225ºC (Alonso-Azcárate et al., 2001, 2006), the anhydrite layers probably flowed
471 during the tectonic deformation associated with the inversion of the basin, while the
472 interbedded carbonates responded in a brittle manner. As a consequence, the carbonate
473 layers broke into prismatic fragments, and were rotated and displaced as the anhydrite

474 groundmass flowed. The final result of this process was the formation of a breccia made
475 up of angular carbonate fragments floating within an anhydrite groundmass.
476 The different degrees of fragment disruption in the breccias of the Oncala Group,
477 varying from very slight displacement to chaotic arrangement (Figs. 8, 9, 10, 11), are
478 probably related with different proportion of sulphate versus carbonate in the original
479 deposits. Moreover, these factors likely controlled which carbonate-evaporitic layers
480 were brecciated and which ones were not. Accordingly, the brecciated layers commonly
481 correspond to stratigraphic levels with large proportion of evaporites relative to
482 carbonate deposits (Figs. 7, 10C, 11A, 11E), and the larger amount of breccias towards
483 the northeastern area of the basin is probably related with the larger amount of
484 evaporitic deposits in that area (Fig. 4B). Similarly, the lower part of the Oncala Group
485 that comprised larger proportion of evaporitic deposits, i.e. the Aguilar del Río Alhama
486 Formation, contains larger amounts of breccias than the upper part of the succession, i.e.
487 the Valdeprado Formation (Figs. 3, 4B), which contained comparatively lower amounts
488 of evaporites. The larger amount of evaporitic deposits probably favoured absorption of
489 much of the deformation that took place in the eastern area of the Cameros Basin during
490 the Alpine inversion (see Casas-Sainz and Simón-Gómez, 1992; Mas et al., 1993;
491 Guimerà et al., 1995) by the Aguilar del Río Alhama Formation (Figs. 2, 13B, 14).
492 The polyharmonic folding that display abundant carbonate breccias (Figs. 9A, 10,
493 13, 14, 15A-D,) is probably caused by compression of carbonate competent layers of
494 different thicknesses embedded in less competent anhydrite (Fig. 13A), as each
495 competent layer is likely to induce its own characteristic wavelength and amplitude
496 (dependant on the thickness of the layer) into the overall fold pattern (cf. Ramsay and
497 Huber, 1987). The less abundant carbonate breccias that show sharp lower and upper
498 contacts (Figs. 8D, 9B) are probably caused by deformation of few layers containing

large proportion of sulphates, underlain and overlain by layers with smaller proportion of sulphates. The large sulphate content of these layers caused them to flow easily under stress and act as shear zones, whereas the underlying and overlying layers remained relatively undeformed.

The preservation of uncalcitized deposits in the lower part of the succession in the easternmost area of the Oncala Group (Figs. 2, 3, 12, 15E-G) provides an excellent opportunity to verify the proposed tectonic sulphate-flow brecciation model. The presence of an alternation of layers of carbonate and gypsum in the easternmost area of the Oncala Group, which display similar features to the calcitized deposits of the rest of the Oncala Group (including intense deformation structures, Figs. 15E, 15G), confirms that the breccias were not the result of evaporite-solution collapse processes. Furthermore, the presence of breccias made up of carbonate fragments floating in a sulphate groundmass (now composed of gypsum) and their close relationship with deformation structures in this uncalcitized area of the Oncala Group (Figs. 12C, 12D, 15F) support that brecciation was caused by tectonically-driven flow of ductile sulphate layers and associated fracturing of brittle carbonate interbeds.

The replacement of anhydrite by quartz and calcite (see section 8.1 above) is interpreted to postdate the deformation of the carbonate-sulphate deposits, which permitted tectonic sulphate flow. Therefore, the current composition of the breccias of the Oncala Group was caused by the anhydrite replacement reactions that postdate carbonate brecciation, which were firstly minor replacement by quartz crystals, and secondly pervasive calcitization in most of the studied area or conversion into secondary gypsum in the easternmost area of the Oncala Group.

Comparable brecciation processes have been described from décollement horizons related to thrust faults by Passeri (1975), Helman and Schreiber (1985), Rouchy et al.

(1987), Jordan and Nüesch (1989), Lugli (2001), and Schreiber and Helman (2005). The readiness of evaporites to flow makes evaporitic units especially favourable to act as décollement zones in thin-skinned fold and thrust belts (Davis and Engelder, 1985; Letouzey et al., 1995), such as the European Jura (Laubsher, 1961; Jordan and Nüesch, 1989), Tuscan Nappe in Northern Apennines (Carmignani and Kligfield, 1990), Dinant Nappe thrust front in Belgium and northern France (Laumondais et al., 1984; Rouchy et al., 1987), or Southeastern Pyrenean thrust front (Sans and Vergés, 1995). In those cases in which the evaporitic décollement horizon contains carbonate interbeds, these carbonate layers are fractured and displaced, resulting in a carbonate-sulphate breccia similar to that of the Oncala Group. Nevertheless, the carbonate breccias of the Oncala Group present several differences with the breccias in the aforementioned literature. First of all, the studied breccias were not related to a thrust zone, but they were developed in a regional tectonic setting characterized by large-scale folds (Gil-Imaz et al., 1990; Gil-Imaz and Pocoví, 1991, 1994). Secondly, the breccias of the Oncala Group show a more complex diagenetic evolution since their sulphate matrix was replaced by quartz and calcite, whereas the breccias in the literature preserved their carbonate-sulphate composition. The absence of preserved evaporites within the studied breccias makes their interpretation more difficult, as the presence of a former ductile lithology is not evident. As a result, the Oncala Group provides a unique example of carbonate breccias caused by the combination of tectonically-driven sulphate-flow carbonate brecciation and subsequent replacement of sulphate by calcite and minor quartz.

9. Concluding remarks: brecciation model and criteria for recognition

549 Carbonate breccias of the Oncala Group were formed as the result of tectonic
550 deformation of alternating brittle carbonate layers and ductile sulphate layers, related to
551 alpine folding of the eastern Cameros Basin. The brecciated beds consisted originally of
552 an alternation of layers of carbonate mudstone and gypsum, which converted to
553 anhydrite during burial. During the Alpine tectonic deformation of the Cameros Basin
554 anhydrite layers flowed, and carbonate layers were broken and displaced, forming a
555 breccia of prismatic carbonate fragments floating in an anhydrite groundmass.
556 Afterwards, the anhydrite was replaced by quartz and calcite.
557 The abundance of alternating carbonate and sulphate deposits in sedimentary
558 successions and the readiness of sulphates to flow under differential stress during burial
559 suggests that similar tectonic sulphate-flow breccias might be common in the geological
560 record. Based on the characteristics of the carbonate breccias of the Oncala Group,
561 useful criteria for identification of similar breccias in the sedimentary record are: 1)
562 evidence of evaporitic layers, which may have been subsequently replaced by non-
563 evaporitic minerals, interbedded with carbonate layers in the original deposits; 2)
564 intraformational origin of the breccia fragments; 3) breccia matrix composed of
565 evaporites, which may have been replaced afterwards; 4) matrix-supported fabric; 5)
566 non-gradational vertical distribution of fabrics; 6) evidence of structural deformation
567 related with the regional tectonic trends.
568
569 **Acknowledgements**
570
571 This work was funded by the Spanish DIGICYT project CGL2011-22709, the
572 “Sedimentary Basin Analysis” Research Group of the Complutense University of
573 Madrid-Madrid Community and a Spanish Department of Education FPU scholarship.

The authors would like to thank two anonymous reviewers for their constructive revisions. We are also grateful to B.C. Schreiber for scientific discussion, her encouragement to write this article and recommendation of useful bibliography, and to A. Jiménez-Díaz and J. Alonso for their help with some terminology on structural geology. We also thank the staff of the Department of Stratigraphy and the Laboratory of Geological Techniques of the Complutense University of Madrid for their technical support.

References

Alonso-Azcárate, J., Barrenecha, J.F., Rodas, M., Mas, R., 1995. Comparative study of the transition between very low grade metamorphism and low grade metamorphism in siliciclastic and carbonate sediments. Early Cretaceous, Cameros Basin (North Spain). Clay Minerals 30, 407-419.

Alonso-Azcárate, J., Rodas, M., Bottrell, S.H., Raiswell, R., Velasco, F., Mas, R., 1999. Pathways and distances of fluid flow during low grade metamorphism: evidence from pyrite deposits of the Cameros Basin, Spain. Journal of Metamorphic Geology 17, 339-348.

Alonso-Azcárate, J., Bottrell, S.H., Tritlla, J., 2001. Sulfur redox reactions and formation of native sulfur veins during low grade metamorphism of gypsum evaporites, Cameros Basin (NE Spain). Chemical Geology 174, 389-402.

Alonso-Azcárate, J., Bottrell, S.H., Mas, J.R., 2006. Synsedimentary versus metamorphic control of S, O and Sr isotopic compositions in gypsum evaporites from the Cameros Basin, Spain. Chemical Geology 234, 46-57.

598 Álvaro, M., Capote, R., Vegas, R., 1979. Un modelo de evolución geotectónica para la
599 Cadena Celtibérica. Acta Geológica Hispánica 14, 172-177.
600 Beales, F.W., Oldershaw, A.E., 1969. Evaporite-Solution Brecciation and Devonian
601 Carbonate Reservoir Porosity in Western Canada. American Association of
602 Petroleum Geologists Bulletin 53, 503-512.
603 Blount, D.N., Moore Jr., C.H., 1969. Depositional and Non-Depositional Carbonate
604 Breccias, Chiantla Quadrangle, Guatemala. Geological Society of America Bulletin
605 80, 429-442.
606 Byrne, T., 1994. Sediment deformation, dewatering and diagenesis: illustrations from
607 selected mélange zones. In: Maltman, A. (Ed.), The geological deformation of
608 sediments. Chapman & Hall, London, pp. 239-260.
609 Cardozo, N., Allmendinger, R.W., 2013. Spherical projections with OSXStereonet.
610 Computers & Geosciences 51, 193-205.
611 Carmignani, L., Kligfield, R., 1990. Crustal extension in the northern Apennines: the
612 transition from compression to extension in the Alpi Apuane core complex.
613 Tectonics 9, 1275-1303.
614 Casas-Sainz, A.M., Simón-Gómez, J.L., 1992. Stress field and thrust kinematics: a
615 model for the tectonic inversion of the Cameros Massif (Spain). Journal of
616 Structural Geology 14, 521-530.
617 Ciarapica, G., Passeri, L., Schreiber, C.B., 1985. Una proposta di classificazione delle
618 evaporiti solfatiche. Geologica romana 24, 219-232.
619 Cossey, S.P.J., 2011. Mass-transport deposits in the upper Paleocene Chicontepec
620 Formation, Mexico. In: Shipp, R.C., Weimer, P., Posamentier, H.W. (Eds.), Mass-
621 Transport Deposits in Deepwater Settings. SEPM Special Publication 96, pp. 269-
622 277.

623 Davis, D.M., Engelder, T., 1985. The role of salt in fold-and-thrust belts.
624 Tectonophysics 119, 67-88.
625 De Bresser, J.H.P., Evans, B., Renner, J., 2002. On estimating the strength of calcite
626 rocks under natural conditions. In: De Meer, S., Drury, M.R., De Bresser, J.H.P.,
627 Pennock, G.M. (eds.), Deformation Mechanisms, Rheology and Tectonics: Current
628 Status and Future Perspectives. Geological Society, London, Special Publication
629 200, pp. 309-329.
630 Dickson, J.A.D., 1966. Carbonate identification and genesis as revealed by staining.
631 Journal of Sedimentary Petrology 36, 491–505.
632 Dozet, S., 1996. Ambrus Beds – Important Key for Interpretation of Neocomian
633 Paleogeography, Sea-Level Changes, Depositional Setting and Tectonics in Suha
634 Krajina Area (Slovenia). Geologija 39, 119-131.
635 Dunham, R.J., 1962. Classification of carbonate rocks according to depositional texture.
636 In: Ham, W.E. (Ed.), Classification of Carbonate Rocks. American Association of
637 Petroleum Geology, Memoir 1, pp. 108-121.
638 Eliassen, A., Talbot, M.R., 2005. Solution-collapse breccias of the Minkinfjellet and
639 Wordiekammen Formations, Central Spitsbergen, Svalbard: a large gypsum
640 palaeokarst system. Sedimentology 52, 775-794.
641 Flügel, E., 2010. Microfacies of Carbonate Rocks: Analysis, Interpretation and
642 Application. Springer, Heidelberg.
643 Gil-Imaz, A., Pocoví, A., 1991. Aplicación del método Rf/Ø al análisis de la
644 deformación finita de los materiales wealdenses de Ágreda (Soria). Geogaceta 9, 27-
645 30.

Gil-Imaz, A., Pocoví, A., 1994. La esquistosidad alpina del extremo NW de la Cadena Ibérica Oriental (Sierra del Moncayo): Distribución, génesis y significado tectónico. Revista Sociedad Geológica de España 7, 91-112.

Gil-Imaz, A., Alba, J., Pocoví, A., 1990. Algunos aspectos de la deformación continua de los materiales mesozoicos del borde noroccidental de la Cordillera Ibérica (Rama Aragonesa): esquistosidad y microestructuras asociadas. Geogaceta 8, 28-30.

Gómez-Fernández, J.C., 1992. Análisis de la Cuenca sedimentaria de los Cameros durante sus etapas iniciales de relleno en relación con su evolución paleogeográfica. Ph.D. Thesis, Complutense University of Madrid, Spain.

Gómez-Fernández, J.C., Meléndez, N., 1994a. Climatic control on Lower Cretaceous sedimentation in a playa-lake system of a tectonically active basin (Huérteles Alloformation, Eastern Cameros Basin, North-Central Spain). Journal of Paleolimnology 11, 91-107.

Gómez-Fernández, J.C., Meléndez, N., 1994b. Estratigrafía de la "Cuenca de los Cameros" (Cordillera Ibérica Noroccidental, N de España) durante el tránsito Jurásico-Cretácico. Revista de la Sociedad Geológica de España 7, 121-139.

González-Acebrón, L., Goldstein, R.H., Mas, R., Arribas, J., 2011. Criteria for recognition of localization and timing of multiple events of hydrothermal alteration in sandstones illustrated by petrographic, fluid inclusion, and isotopic analysis of the Tera Group, Northern Spain. International Journal of Earth Sciences: Geologische Rundschau 100, 1811-1826.

González-Acebrón, L., Goldstein, R.H., Mas, R., Arribas, J., 2012. Easily altered minerals and reequilibrated fluid inclusions provide extensive records of fluid and thermal history: gypsum pseudomorphs of the Tera Group, Tithonian-Berriasian, Cameros Basin. Central European Journal of Geosciences 4, 246-260.

671 Grohmann, C.H., Campanha, G.A.C., 2010. OpenStereo: open source, cross-platform
672 software for structural geology analysis. AGU 2010 Fall Meeting, San Francisco.
673 Guimerà, J., Alonso, A., Mas, R., 1995. Inversion of an extensional-ramp basin by a
674 newly formed thrust: the Cameros Basin (N Spain). In: Buchanan, J.G., Buchanan,
675 P.G. (Eds.), Basin Inversion. Geological Society, London, Special Publication 88,
676 pp. 433-453.
677 Helman, M.L., Schreiber, B.C., 1985. Permian evaporite deposits of the Italian Alps
678 (Dolomites): the development of unusual and significant fabrics. In: Schreiber, B.C.,
679 Harner, L. (Eds.), Sixth International Symposium on Salt, vol. 1. Salt Institute,
680 Alexandria, Virginia, pp. 57–66.
681 Hoffman, P.F., Calver, C.R., Halverson, G.P., 2009. Cottons Breccia of King Island,
682 Tasmania: Glacial or non-glacial, Cryogenian or Ediacaran? Precambrian Research
683 172, 311-322.
684 Holliday, D.W., 1970. The petrology of secondary gypsum rocks: a review. Journal of
685 Sedimentary Petrology 40, 734-744.
686 Jauzein, A., 1974. Les données sur le système $CaSO_4$, H_2O et leurs implications
687 géologiques. Revue de Géographie Physique et de Géologie Dynamique (2) 16, 151-
688 159.
689 Jordan, P., Nüesch, R., 1989. Deformation Structures in the Muschelkalk Anhydrites of
690 the Schafisheim Well (Jura Overthrust, Northern Switzerland). Eclogae geologicae
691 Helvetiae 82, 429-454.
692 Jowett, E.C., Cathles III, L.M., Davis, B.W., 1993. Predicting Depths of Gypsum
693 Dehydration in Evaporitic Sedimentary Basins. American Association of Petroleum
694 Geologists Bulletin 77, 402-413.

695 Kendall, A.C., 1992. Evaporites. In: Walker, R.G., and James, N.P. (Eds.), Facies
696 Models: Response to Sea Level Change. Geological Association of Canada, St.
697 John's, Newfoundland, pp. 375–409.
698 King, P.R., Ilg, B.R., Arnot, M.A., Browne, G.H., Strachan, L.J., Crundwell, M., Helle,
699 K., 2011. Outcrop and seismic examples of mass-transport deposits from a Late
700 Miocene deep-water succession, Taranaki Basin, New Zealand. In: Shipp, R.C.,
701 Weimer, P., Posamentier, H.W. (Eds.), Mass-Transport Deposits in Deepwater
702 Settings. SEPM Special Publication 96, pp. 311-348.
703 Laubscher, H.P. (1961): Die Fernschubhypothese del Jurafaltung. Eclogae geologicae
704 Helvetiae 54, 221-281.
705 Laumondais, A., Rouchy, J.M., Groessens, E., 1984. Importance des formations
706 anhydritiques dinantiennes pour l'interprétation paléogéographique et structurale du
707 domaine varisque d'Europe septentrional. Comptes Rendus de l'Academie de
708 Sciences 298, 411-414.
709 Letouzey, J., Colletta, B., Vially, R., Chermette, J.C. (1995): Evolution of Salt-Related
710 Structures in Compressional Settings. In: Jackson, M.P.A., Roberts, D.G., Snelson,
711 S. (Eds.), Salt tectonics: a global perspective. AAPG Memoir 65, pp. 41-60.
712 Loucks, R.G., Mescher, P.K., McMechan, G.A., 2004. Three-dimensional architecture
713 of a coalesced, collapsed paleocave system in the Lower Ordovician Ellenburger
714 Group, central Texas. American Association of Petroleum Geologists Bulletin 88,
715 545-564.
716 Lugli, S., 2001. Timing of post-depositional events in the Burano Formation of the
717 Secchia valley (Upper Triassic, Northern Apennines), clues from gypsum–anhydrite
718 transitions and carbonate metasomatism. Sedimentary Geology 140, 107–122.

MacDonald, G.J.F., 1953. Anhydrite-gypsum equilibrium relations. American Journal of Science 251, 884-898.

Magee, J.W., 1991. Late Quaternary lacustrine, groundwater, aeolian and pedogenic gypsum in the Prungle Lakes, southeastern Australia. Palaeogeography, Palaeoclimatology, Palaeoecology 84, 3-42.

Mantilla-Figueroa, L.C., Casquet, C., Galindo, C., Mas, J.R., 2002. El metamorfismo hidrotermal cretácico y paleógeno en la Cuenca de Cameros (Cordillera Ibérica, España). Zubía 14, 143-154.

Martinsen, O., 1994. Mass movements. In: Maltman, A. (Ed.), The geological deformation of sediments. Chapman & Hall, London, pp. 127-165.

Mas, R., Alonso, A., Guimerà, J., 1993. Evolución tectonosedimentaria de una cuenca extensional intraplaca: la cuenca finijurásica-eocretácica de Los Cameros (La Rioja-Soria). Revista de la Sociedad Geológica de España 6, 129-144.

Mas, R., Benito, M.I., Arribas, J., Serrano, A., Guimerà, J., Alonso, A., Alonso-Azcarate, J., 2002. La Cuenca de Cameros: desde la extensión finijurásica-eocretácica a la inversión terciaria – implicaciones en la exploración de hidrocarburos. Zubía 14, 9-64.

Mas, R., García, A., Salas, R., Meléndez, A., Alonso, A., Aurell, M., Bádenas, B., Benito, M.I., Carenas, B., García-Hidalgo, J.F., Gil, J., Segura, M., 2004. Segunda fase de rifting: Jurásico Superior-Cretácico Inferior. In: Vera, J.A. (Ed.), Geología de España. SGE-IGME, Madrid, pp. 503-510.

Mas, R., Benito, M.I., Arribas, J., Alonso, A., Arribas, M.E., Lohmann, K.C., González-Acebrón, L., Hernán, J., Quijada, E., Suarez, P., Omodeo, S., 2011. Evolution of an intra-plate rift basin: the Latest Jurassic-Early Cretaceous Cameros Basin (Northwest Iberian Ranges, North Spain). In: Arenas, C., Pomar, L., Colombo, F.

744 (Eds.), Post-Meeting Field trips 28th IAS Meeting, Zaragoza. Geo-guías 8, pp. 117-
745 154.
746 Mata, M.P., Casas, A.M., Canals, A., Gil, A., Pocoví, A., 2001. Thermal history during
747 Mesozoic extension and Tertiary uplift in the Cameros Basin, northern Spain. Basin
748 Research 13, 91-111.
749 McWhae, J.R.H., 1953. The Carboniferous Breccias of Billefjorden, Vestspitsbergen.
750 Geological Magazine 90, 287–298.
751 Meléndez, N., Gómez-Fernández, J.C., 2000. Continental Deposits of the Eastern
752 Cameros Basin (Northern Spain) During Tithonian-Berriasian Time. In: Gierlowski-
753 Kordesch, E.H., Kelts, K.R. (Eds.), Lake basins through space and time. AAPG
754 Studies in Geology 6, pp. 263-278.
755 Middleton, G.V., 1961. Evaporite solution breccias from the Mississippian of southwest
756 Montana. Journal of Sedimentary Petrology 31, 189-195.
757 Moretti, M., Owen, G., Tropeano, M., 2011. Soft-sediment deformation induced by
758 sinkhole activity in shallow marine environments: A fossil example in the Apulian
759 Foreland (Southern Italy). Sedimentary Geology 235, 331-342.
760 Müller, W.H., Briegel, U., 1978. The rheological behaviour of polycrystalline anhydrite.
761 Eclogae geologicae Helvetiae 71, 397-407.
762 Müller, W.H., Schmid, S.M., Briegel, U., 1981. Deformation experiments on anhydrite
763 rocks of different grain sizes: rheology and microfabric. Tectonophysics 78, 527-
764 543.
765 Norton, W.H., 1917. A Classification of Breccias. The Journal of Geology 25, 160-194.
766 Omodeo-Salè, S., Guimerà, J., Arribas, J., Mas, R., 2014. Tectono-stratigraphic
767 evolution of an inverted extensional basin: the Cameros Basin (North of Spain).
768 International Journal of Earth Sciences. doi: 10.1007/s00531-014-1026-5

769 Ortí, F., 2010. Evaporitas: introducción a la sedimentología evaporítica. In: Arche, A.
770 (Ed.), Sedimentología. Del Proceso Físico a la Cuenca Sedimentaria. Consejo
771 Superior de Investigaciones Científicas, Madrid, pp. 675–769.
772 Passeri, L., 1975. L'ambiente deposizionale della formazione evaporitica nel quadro
773 della paleogeografia del norico Tosco-Umbro-Marchigiano. Bolletino della Società
774 Geologica Italiana 94, 231–268.
775 Papaioanou, F. P., Carotsieris, Z., 1993. Dolomitization patterns in Jurassic-Cretaceous
776 dissolution-collapse breccias of Mainalon Mountain. Carbonates and Evaporites 8,
777 9–22.
778 Payros, A., Pujalte, V., Orue-Etxebarria, X., 1999. The South Pyrenean Eocene
779 carbonate megabreccias revisited: new interpretation based on evidence from the
780 Pamplona Basin. Sedimentary Geology 125, 165-194.
781 Peryt, T.M., Kasprzyk, A., 1992. Earthquake-induced resedimentation in the Badenian
782 (middle Miocene) gypsum of southern Poland. Sedimentology 39, 235-249.
783 Pierre, C., Rouchy, J.M., 1988. Carbonate replacements after sulfate evaporites in the
784 middle Miocene of Egypt. Journal of Sedimentary Petrology 58, 446-456.
785 Posamentier, H.W., Martinsen, O.J., 2011. The character and genesis of submarine
786 mass-transport deposits: insights from outcrop and 3D seismic data. In: Shipp, R.C.,
787 Weimer, P., Posamentier, H.W. (Eds.), Mass-Transport Deposits in Deepwater
788 Settings. SEPM Special Publication 96, pp. 7-38.
789 Quijada, I.E., Suarez-Gonzalez, P., Benito, M.I., Mas, R., 2013a. Depositional depth of
790 laminated carbonate deposits: insights from the Lower Cretaceous Valdeprado
791 Formation (Cameros Basin, northern Spain). Journal of Sedimentary Research 83,
792 241-257.

793 Quijada, I.E., Suarez-Gonzalez, P., Benito, M.I., Mas, R., 2013b. New insights on
794 stratigraphy and sedimentology of the Oncala Group (eastern Cameros Basin):
795 implications for the paleogeographic reconstruction of NE Iberia at Berriasian times.
796 Journal of Iberian Geology 39, 313-334.
797 Quijada, I.E., Suarez-Gonzalez, P., Benito, M.I., Mas, R., 2014. Tidal versus continental
798 sandy-muddy flat deposits: evidence from the Oncala Group (Early Cretaceous, N
799 Spain). In: Tessier, B., Reynaud, J.Y. (Eds.). International Association of
800 Sedimentologists Special Publication 48 (in press).
801 Ramsay, J.G., Huber, M.I., 1987. The techniques of modern Structural Geology, volume
802 2: Folds and Fractures. Academic Press, London.
803 Richter, D.K., Füchtbauer, H., 1981. Merkmale und Genese von Breccien und ihre
804 Bedeutung im Mesozoikum von Hydra (Griechenland). Zeitschrift der Deutschen
805 Geologischen Gesellschaft 132, 451-501.
806 Rouchy, J.M., Laumondais, A., Groessens, E., 1987. The lower Carboniferous (Visean)
807 evaporites in northern France and Belgium: depositional, diagenetic and
808 deformational guides to reconstruct a disrupted evaporitic basin. In Peryt, T.M.
809 (Ed.), Evaporite Basins. Lecture Notes in Earth Sciences 13, pp. 31-67.
810 Salas, R., Guimerà, J., Mas, R., Martín-Closas, C., Meléndez, A., Alonso, A., 2001.
811 Evolution of the Mesozoic Central Iberian Rift System and its Cainozoic inversion
812 (Iberian Chain). In: Ziegler, P.A., Cavazza, W., Robertson, A.F.H., Crasquin-
813 Soleau, S. (Eds.), Peri-Tethys Memoir 6: Peri-Tethyan Rift/Wrench Basins and
814 Passive Margins. Mémoires du Muséum National d'Histoire Naturelle 186, pp. 145-
815 185.
816 Salomon, J., 1982. El Cretácico inferior de Cameros-Castilla. In: García, A. (Ed.), El
817 Cretácico de España. Universidad Complutense de Madrid, Madrid, pp. 345-387.

818 Sans, M., Vergés, J., 1995. Fold development related to contractional salt tectonics:
819 southeastern Pyrenean thrust front, Spain. In: Jackson, M.P.A., Roberts, D.G.,
820 Snelson, S. (Eds.), Salt tectonics: a global perspective. AAPG Memoir 65, pp. 369-
821 378.
822 Schreiber, B.C., Helman, M.L., 2005. Criteria for distinguishing primary evaporite
823 features from deformation features in sulphate evaporites. Journal of Sedimentary
824 Research 75, 525-533.
825 Schudack, U., Schudack, M., 2009. Ostracod biostratigraphy in the Lower Cretaceous
826 of the Iberian chain (eastern Spain). Journal of Iberian Geology 35, 141-168.
827 Shearman, D.J., 1983. Syndepositional and Late Diagenetic Alteration of Primary
828 gypsum to Anhydrite. In: Schreiber, B.C., Harner, L. (Eds.), Sixth International
829 Symposium on Salt, vol. 1. Salt Institute, Alexandria, Virginia, pp. 41-55.
830 Spalluto, L., Moretti, M., Festa, V., Tropeano, M., 2007. Seismically-induced slumps in
831 Lower-Maastrichtian peritidal carbonates of the Apulian Platform (southern Italy).
832 Sedimentary Geology 196, 81-98.
833 Stanton Jr., R.J., 1966. The Solution Brecciation Process. Geological Society of
834 America Bulletin 77, 843-848.
835 Stow, D.A.V., Reading, H.G., Collinson, J.D., 1996. Deep seas. In: Reading, H.G.
836 (Ed.), Sedimentary Environments: Processes, Facies and Stratigraphy. Blackwell
837 Science, Oxford, pp. 395-453.
838 Suarez-Gonzalez, P., Quijada, I.E., Benito, M.I., Mas, R., 2013. Eustatic versus tectonic
839 control in an intraplate rift basin (Leza Fm, Cameros Basin). Chronostratigraphic
840 and paleogeographic implications for the Aptian of Iberia. Journal of Iberian
841 Geology 39, 285-312.

842 Suarez-Gonzalez, P., Quijada, I.E., Benito, M.I., Mas, R., Merinero, R., Riding, R.,
843 2014. Origin and significance of lamination in Lower Cretaceous stromatolites and
844 proposal for a quantitative approach. Sedimentary Geology 300, 11–27
845 Suarez-Gonzalez, P., Quijada, I.E., Benito, M.I., Mas, R., 2014. Do stromatolites need
846 tides to trap ooids? Insights from oolitic stromatolites of a Cretaceous system of
847 coastal-wetlands. In: Tessier, B., Reynaud, J.Y. (Eds.). International Association of
848 Sedimentologists Special Publication 48, in press.
849 Swennen, R., Viaene, W., Cornelissen, C., 1990. Petrography and geochemistry of the
850 Belle Roche breccia (lower Visean, Belgium): evidence for brecciation by evaporite
851 dissolution. Sedimentology 37, 859-878.
852 Tucker, M.E., 2011. Sedimentary Rocks in the Field: a practical guide. Wiley-
853 Blackwell, Chichester.
854 Vegas, R. Banda, E., 1982. Tectonic framework and Alpine evolution of the Iberian
855 Peninsula. Earth Evolution Sciences 4, 320-343.
856 Vlahovic, I., Mandic, O., Mrinjek, E., Bergant, S., Cosovic, V., de Leeuw, A., Enos, P.,
857 Hrvatovic, H., Maticec, D., Miksa, G., Nemec, W., Pavelic, D., Pencinger, V., Velic,
858 I., Vranjkovic, A., 2012. Marine to continental depositional systems of Outer
859 Dinarides foreland and intra-montane basins (Eocene-Miocene, Croatia and Bosnia
860 and Herzegovina. Journal of Alpine Geology 54, 405-470.
861 Warren, J.K., 2006. Evaporites: Sediments, Resources and Hydrocarbons. Springer,
862 Berlin.
863 Woodcock, N.H., 1976. Structural style in slump sheets: Ludlow Series, Powys, Wales.
864 Journal of the Geological Society of London 132, 399-415.
865
866

Figure 1

Click here to download high resolution image

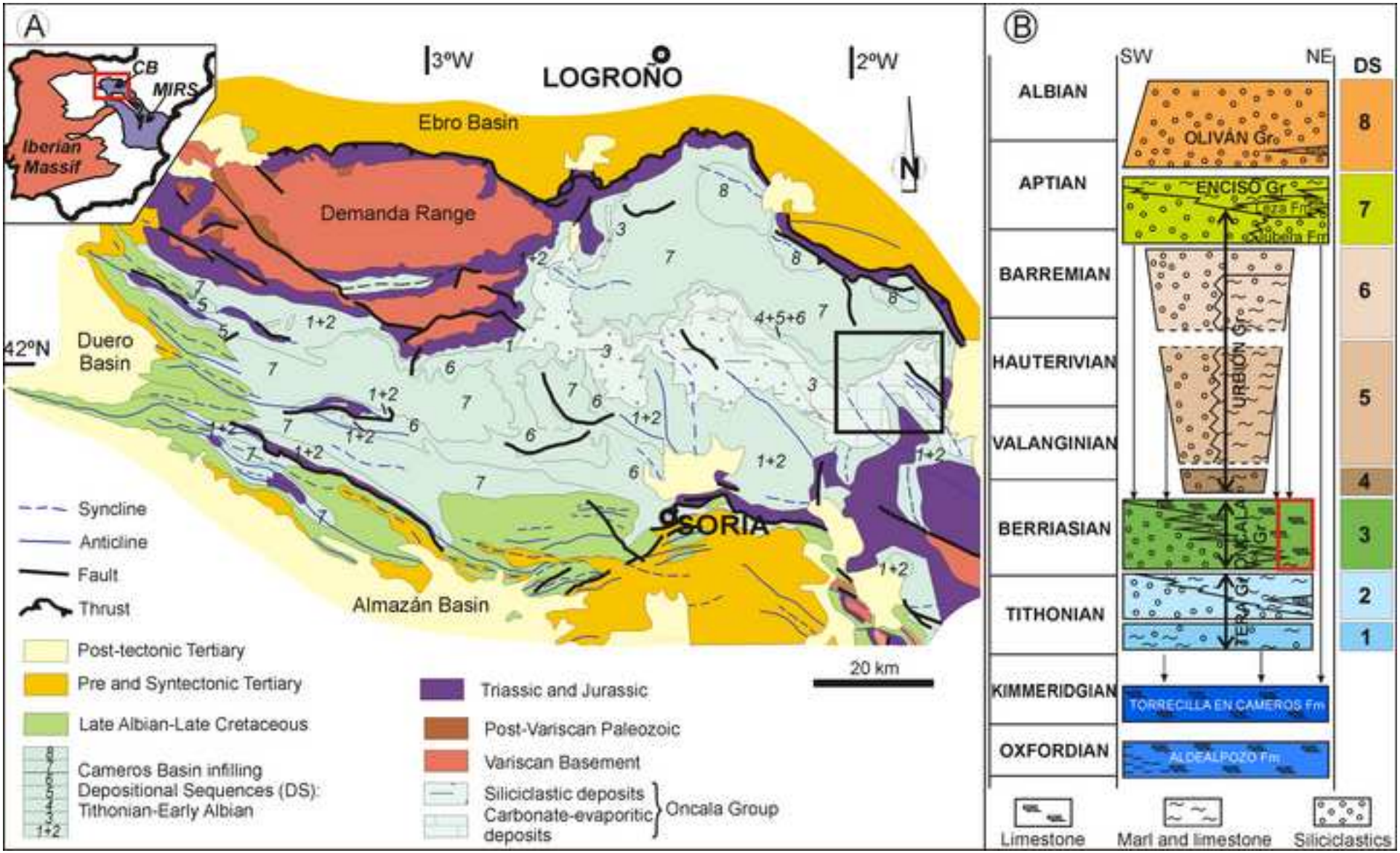

Figure 2

Click here to download high resolution image

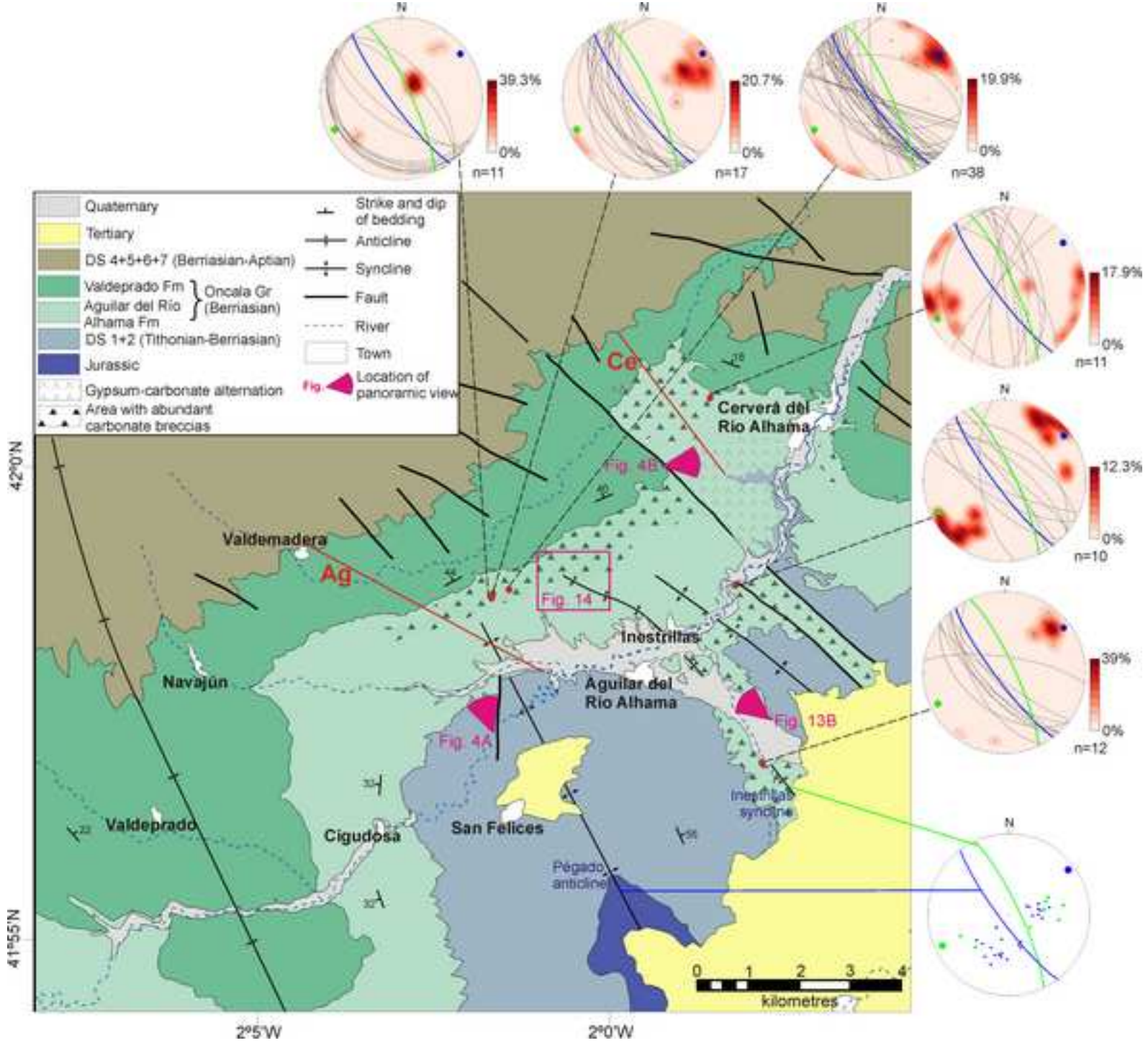

Figure 3

Click here to download high resolution image

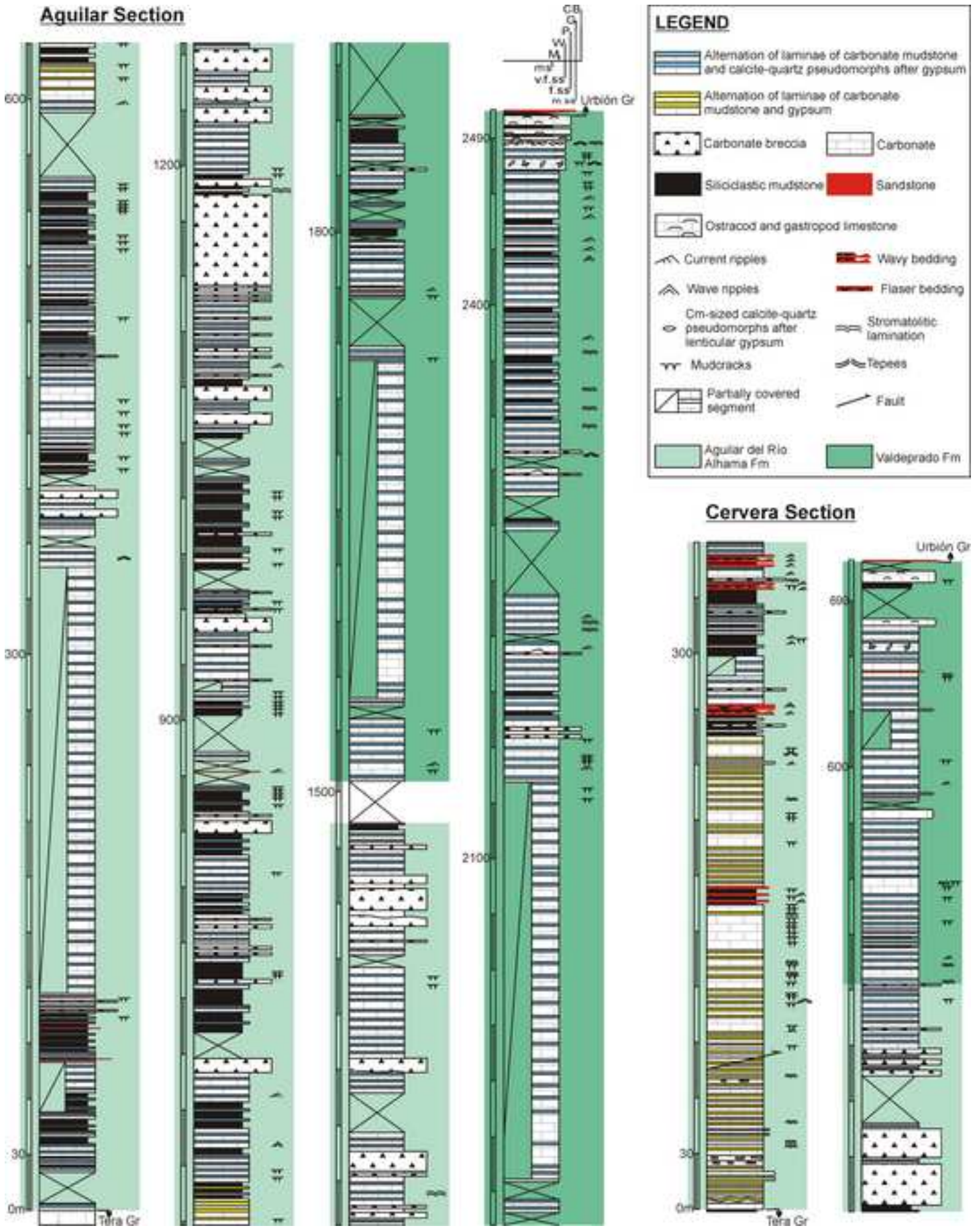

Figure 7

Click here to download high resolution image

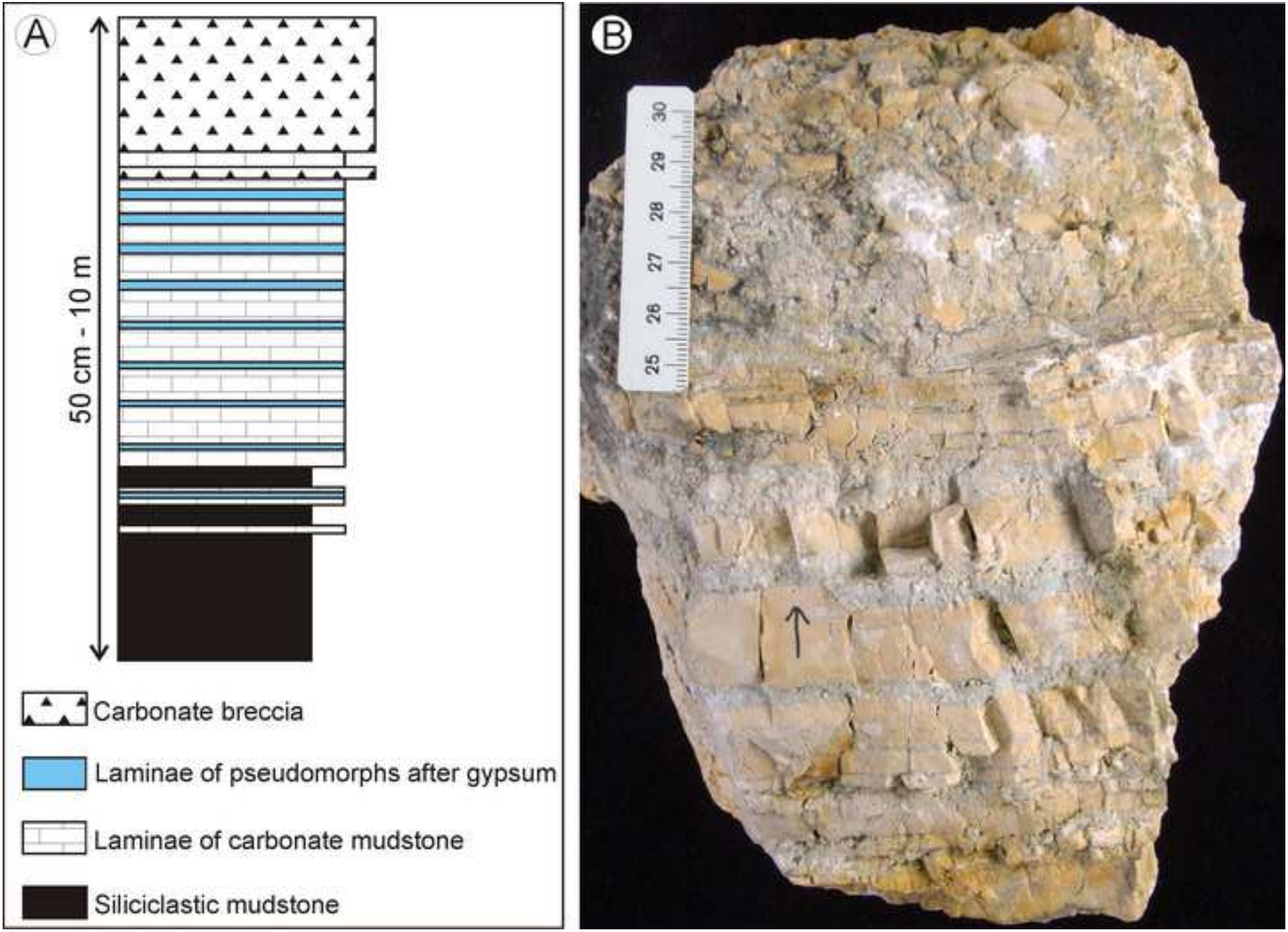

Figure 8

Click here to download high resolution image

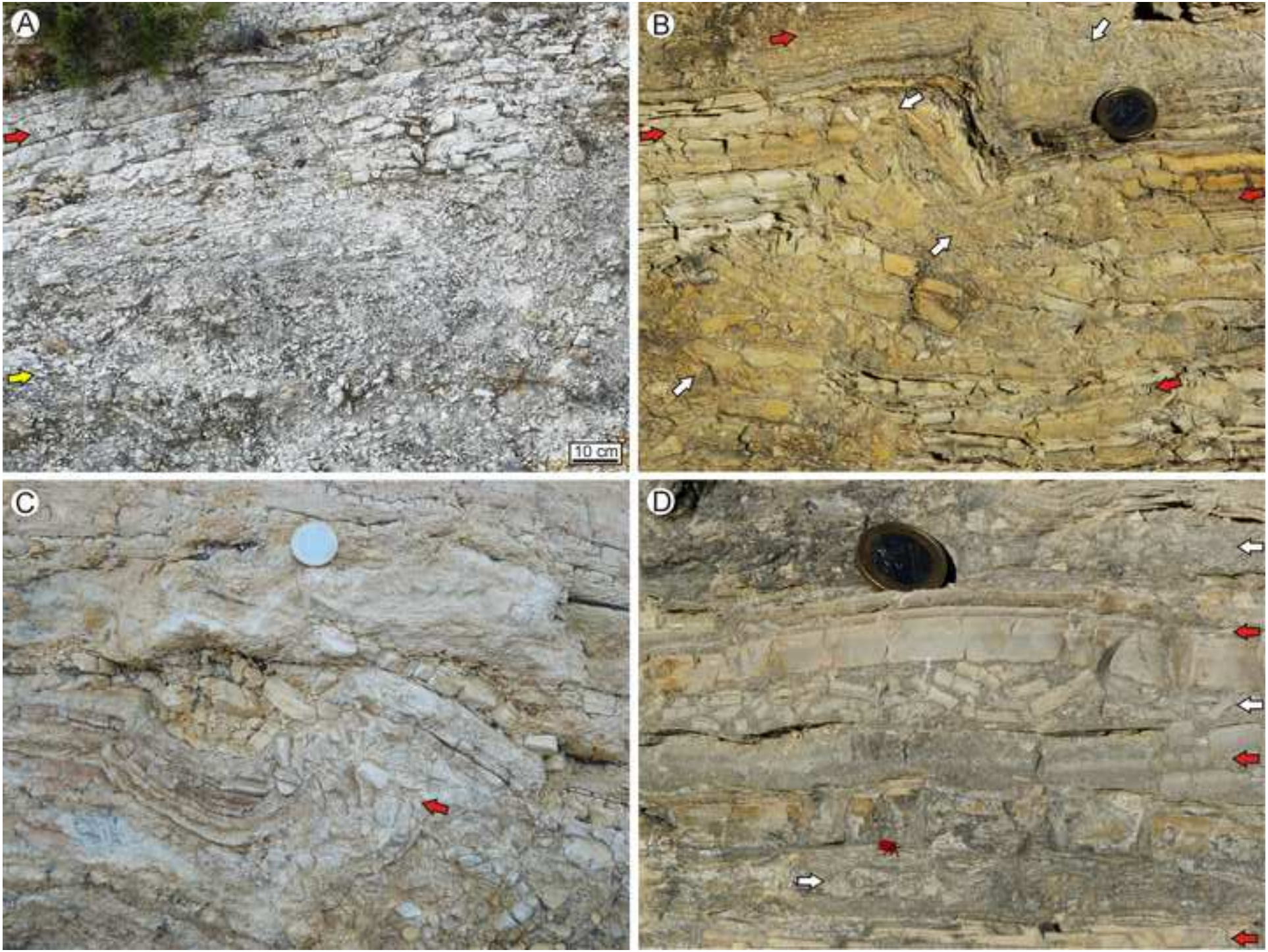

Figure 9

Click here to download high resolution image

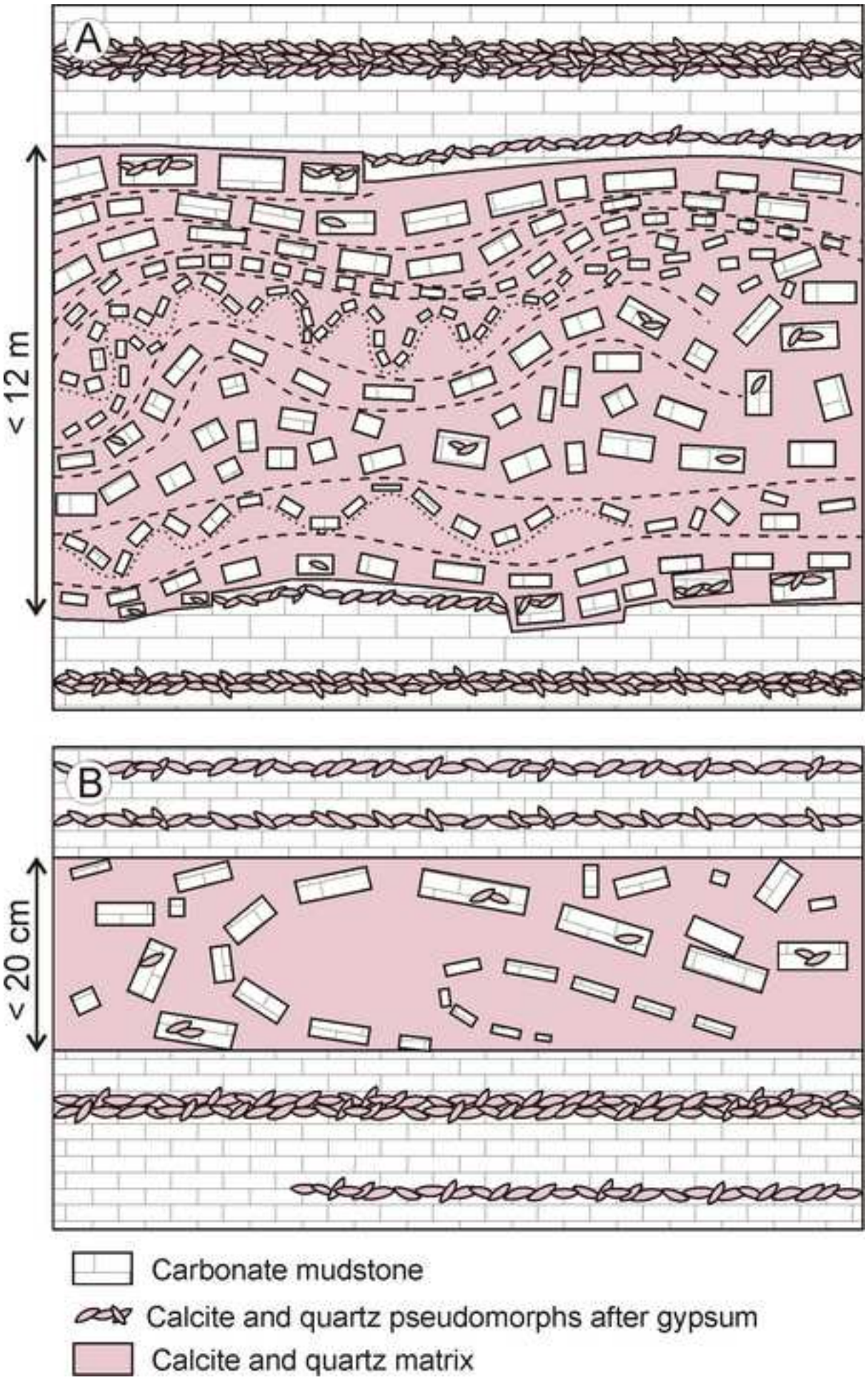

Figure 10

Click here to download high resolution image

Figure 11
Click here to download high resolution image

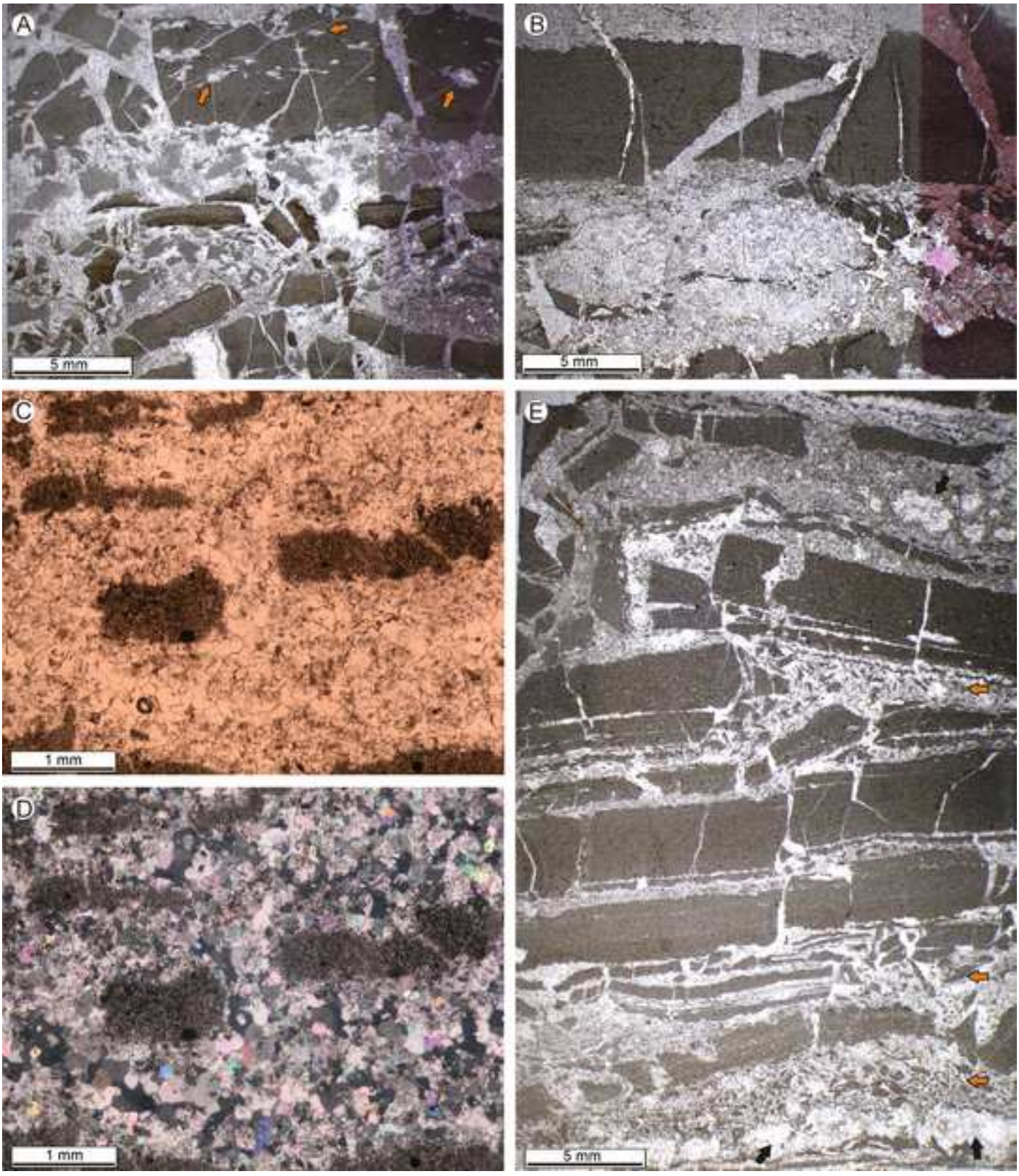

Figure 12

Click here to download high resolution image

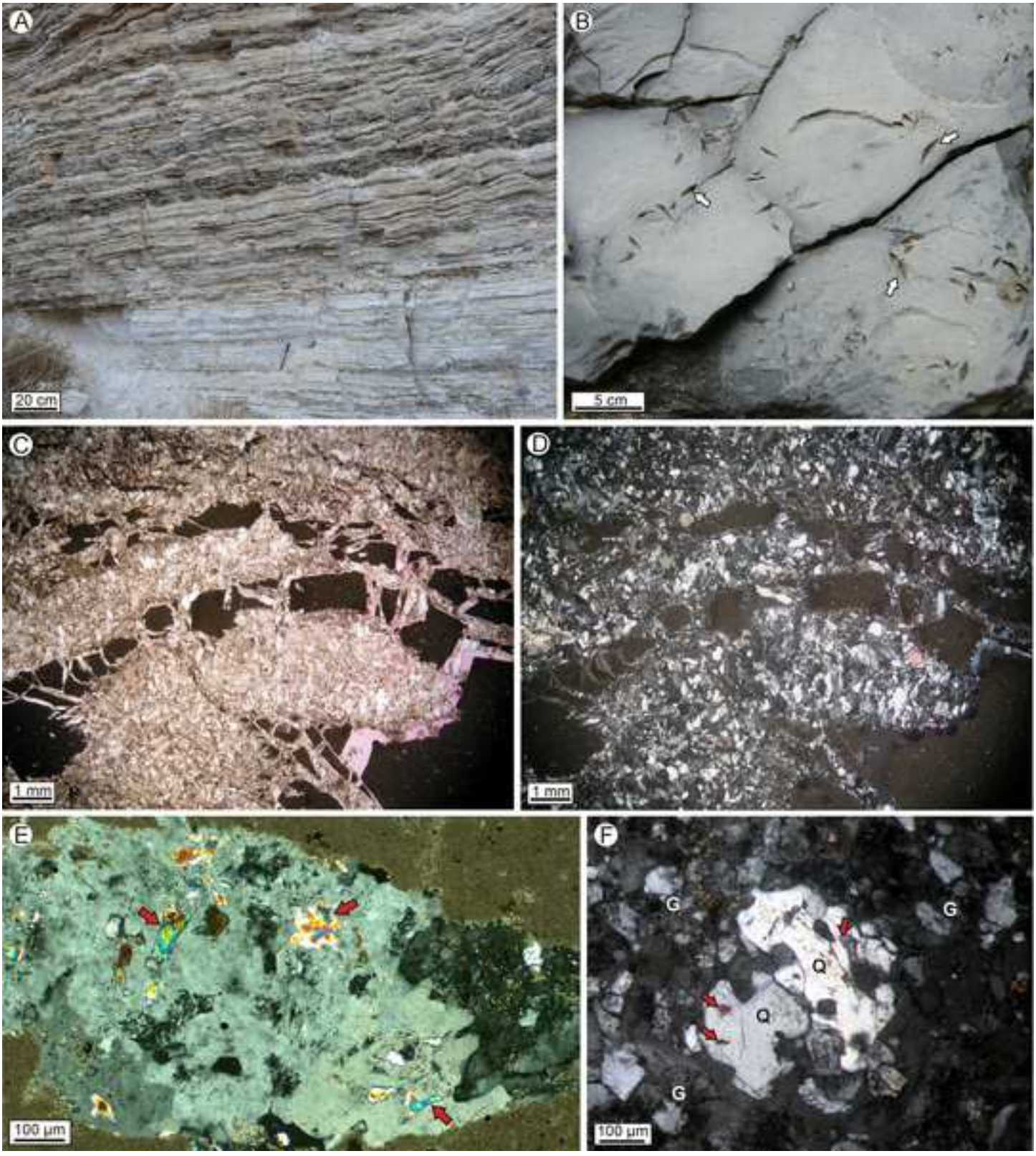

Figure 13

Click here to download high resolution image

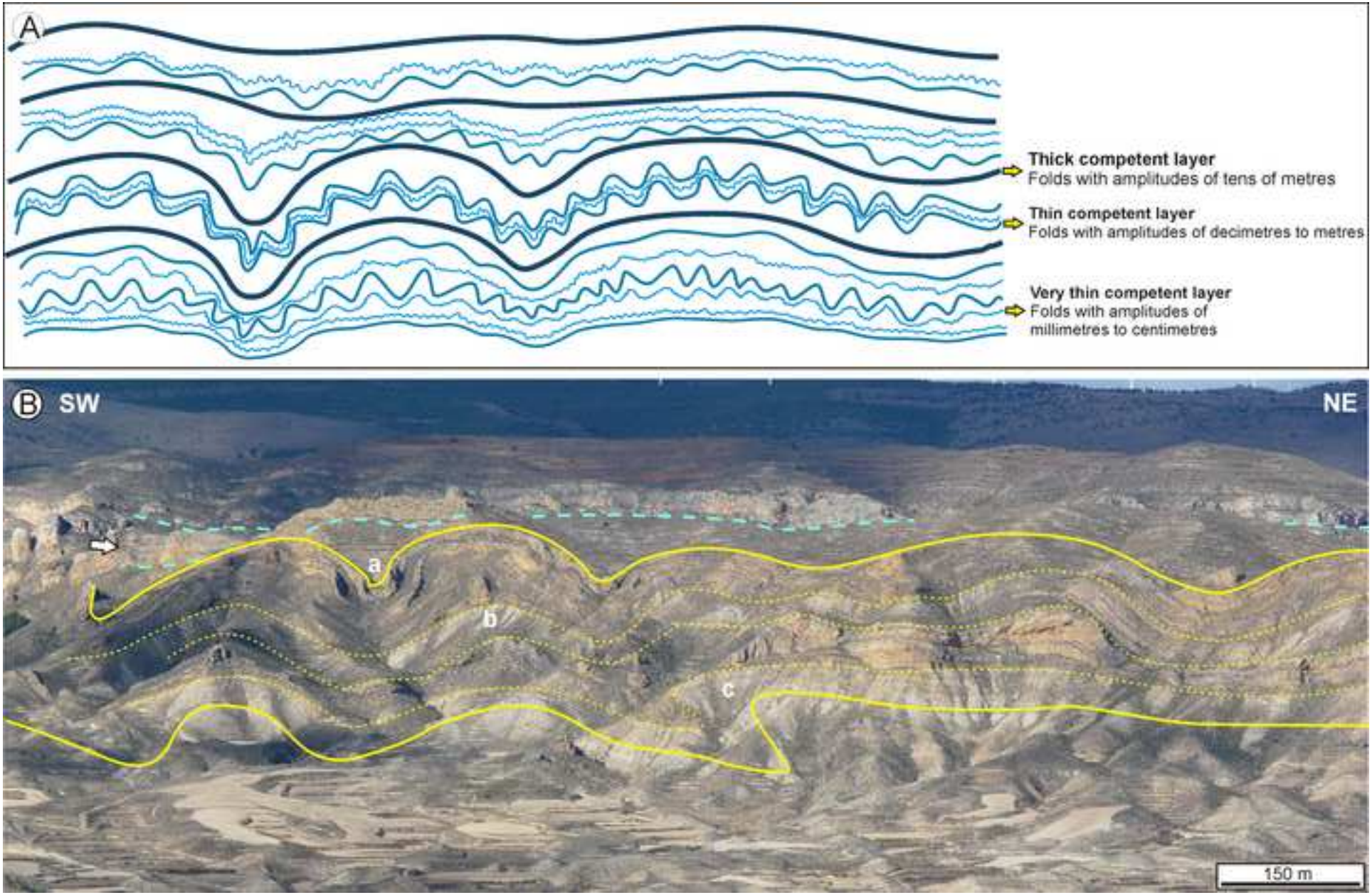

Figure 14

Click here to download high resolution image

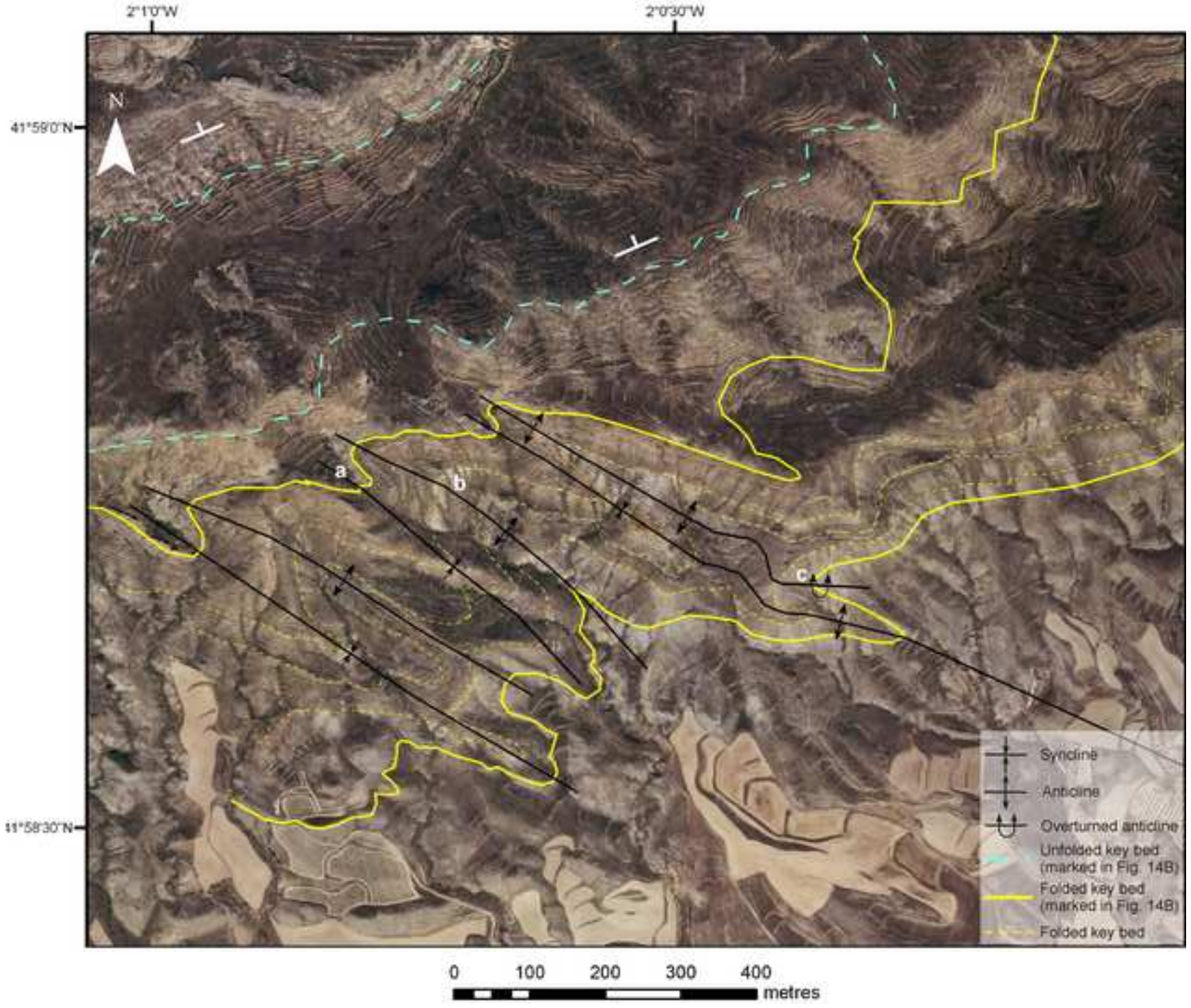

Figure 15

Click here to download high resolution image

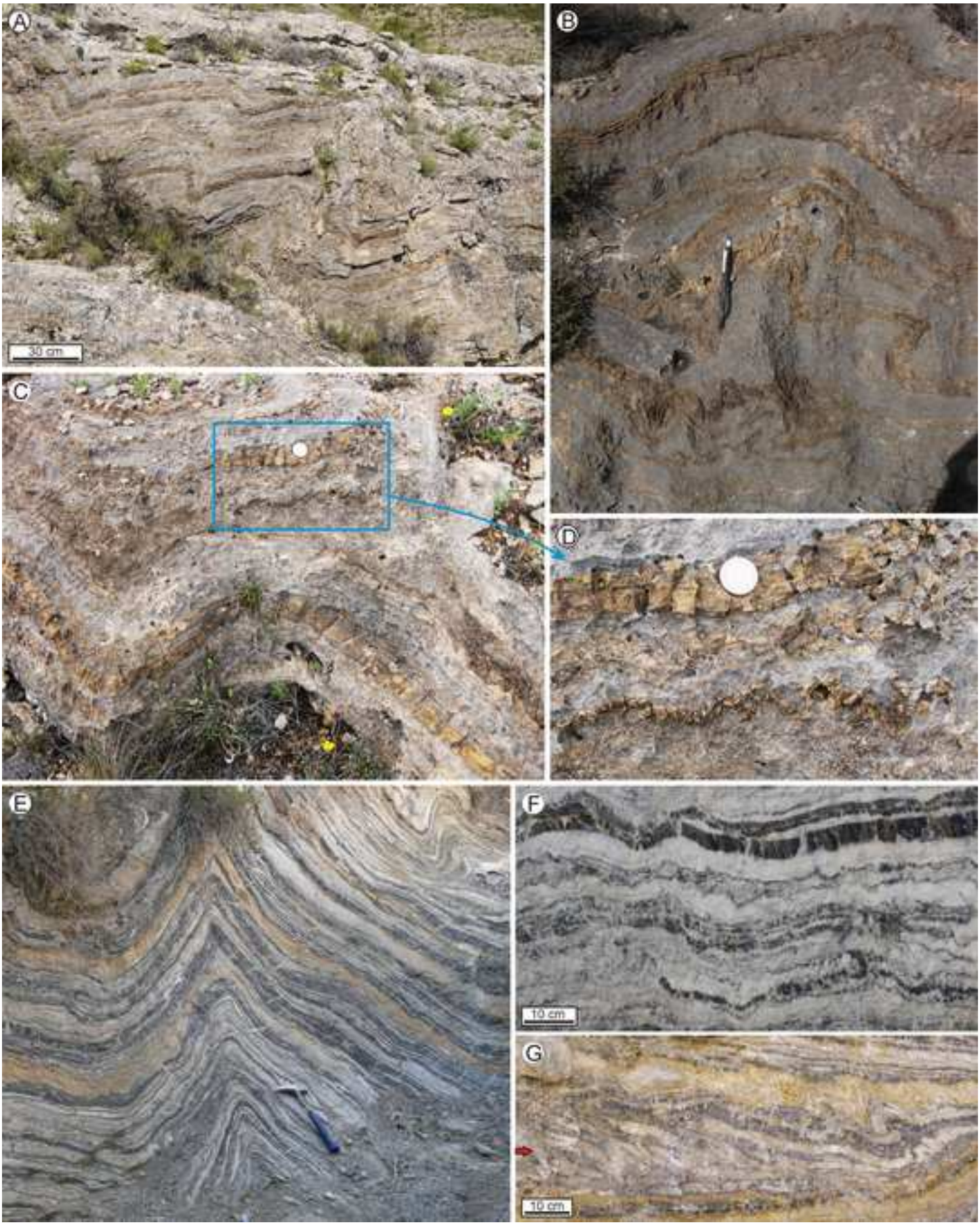

Figure 16

Click here to download high resolution image

	Tectonic sulphate-flow breccia	Evaporite-solution collapse breccia	Slump breccia
	Tectonic deformation of alternating brittle carbonate layers and ductile sulphate layers	Collapse of beds subsequent to the removal of soluble evaporites	Downslope transport of sediments
		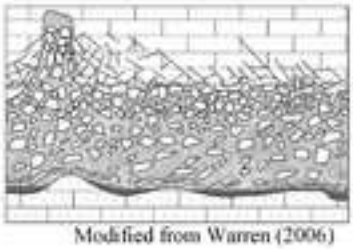 Modified from Warren (2006)	
Stratification and organization of fragments	Stratigraphic order of the former intra-evaporite beds is commonly preserved	Stratigraphic order of the former intra-evaporite beds is commonly preserved	Significant internal distortion of the bedding
	Fragments vary from slightly displaced to chaotic	Displacement of fragments decreases upwards	Common normal or inverse grading
Boundaries and relationship to adjacent rocks	Mostly irregular lower and upper contacts, and gradual lateral change to unbrecciated layers of similar composition	Sharp, planar, continuous lower contact, and gradational upper contact	Sharp lower and upper contacts that truncate the structures underneath
Related lithologies	(Vanished) evaporites	(Vanished) evaporites	Fine-grained sediments
Relationship with deformation structures	Close relationship with deformed deposits. Folds within the breccias	Deformation occurs only when solution takes place in unconsolidated sediments. Elongated conical zones of sinking	(Overturned and recumbent) folds, boudins, microfaults, internal shear surfaces and faults within slump beds. Upper extensional zone and downslope contractional zone indicating lateral mass movement
	Deformation related with regional tectonic structures.	Deformation unrelated with regional tectonic structures, but caused by vertical pressure	Deformation unrelated with regional tectonic structures
	Thickness of deformed sequences independent from depositional depth		Thickness of deformed sequences smaller than depositional depth
Fragments	Angular (rectangular prisms)	Angular or subangular	All degrees of roundness
	Derived from layers interbedded with evaporites	Derived from layers overlying or interbedded with evaporites	Mixture of material transported from adjacent areas
Matrix	(Replaced) evaporites	Cements and/or fine-grained matrix resulting from internal brecciation of coarser fragments	Fine-grained sedimentary matrix, commonly brought together with the clasts
Fabric	Mostly matrix-supported	Clast- or matrix-supported	Usually clast-supported
		Clast support increases upwards	
Sedimentary structures	None	None	Burrows, dewatering structures and/or sand volcanoes at the top
Other features		Footwall surface covered by insoluble residues	

FIGURE AND TABLE CAPTIONS

Fig. 1. (A) Geological map of the Cameros Basin and location within the Iberian Peninsula. Note that the Oncala Group (Depositional Sequence 3) contains laterally related siliciclastic and carbonate-evaporitic deposits. The black rectangle marks the mapped area in Fig. 2. Modified from Mas et al. (2002). "CB" = Cameros Basin, "MIRS" = Mesozoic Iberian Rift System. (B) Stratigraphic framework and depositional sequences (DS) filling the eastern Cameros Basin. The focus of this study, the eastern deposits of the Oncala Group, is highlighted with a red rectangle. Modified from Mas et al. (2004). "Gr" = Group, "Fm" = Formation.

Fig. 2. Detailed geological map of the study area with stereographic projections depicting the attitude of the folds in the area (Schmidt's projection, lower hemisphere, equiareal net). Notice that carbonate breccia layers are most abundant in the northeastern area of the Aguilar del Río Alhama Formation, and that the lower part of the Oncala Group in the easternmost area of the basin contains an alternation of gypsum and carbonate layers. The red line marks the position of measured stratigraphic sections of the Oncala Group. "Ag" = Aguilar section, "Ce" = Cervera section, "Fm" = Formation, "Gr" = Group, "DS" = Depositional Sequence. The stereographic projection in the lower right area of the figure shows the axial planes and poles of the Pégado anticline (blue) and Inestrillas syncline (green), calculated from poles to bedding (small dots) using Stereonet 8. The other stereographic projections (plotted using OpenStereo) show the axial planes, poles and density contours of poles of the decimetre to metre-scale folds within the Oncala Group (red dots in the map indicate the location of the measurement sites). The axial planes and poles of the Pégado

anticline (blue) and Inestrillas syncline (green) have been represented in the stereographic projections of the folds within the Oncala Group to facilitate comparison. Note that the folds within the Oncala Group strike similarly to the regional tectonic structures.

Fig. 3. Synthetic stratigraphic sections of Aguilar and Cervera (see Fig. 2 for location). Notice that the Oncala Group consists mainly of alternating laminae of carbonate mudstone and calcite and quartz pseudomorphs after gypsum, but the lowermost part of the Cervera section and few metres of the Aguilar section contain alternating carbonate mudstone and gypsum. Note that the carbonate breccias are much more abundant in the Aguilar del Río Alhama Formation than in the Valdeprado Formation. "ms" = siliciclastic mudstone, "v.f.ss" = very fine-grained sandstone, "f.ss" = fine-grained sandstone, "m.ss" = medium-grained sandstone, "M" = carbonate mudstone, "W" = wackestone, "P" = packstone, "G" = grainstone, "CB" = carbonate breccia, "Fm" = Formation.

Fig. 4. (A) Southwest-Northeast panoramic photograph of the Aguilar del Río Alhama Formation in the eastern area of the Cameros Basin (see Fig. 2 for location). Competent layers in this photograph consist of carbonate breccias and alternating layers of carbonate mudstone and calcite-quartz pseudomorphs after gypsum. Incompetent layers are composed of siliciclastic mudstone and alternating layers of carbonate mudstone and calcite-quartz pseudomorphs after gypsum. The arrow indicates the stratigraphic level with polyharmonic folds shown in Figs. 15A-D. The stratigraphic level marked by the arrow corresponds laterally to that marked in Fig. 13A. (B) North-South panoramic photograph of the Oncala Group in the easternmost area of the Cameros Basin (see Fig.

2 for location). Competent layers consist mainly of carbonate breccias. Note that the carbonate breccias thin southwards eventually disappearing. Yellow line indicates the contact of the Oncala Group with the overlying Urbión Group, and red line marks the contact between the Aguilar del Río Alhama Formation and the Valdeprado Formation (see Fig. 2). Notice that carbonate breccias are much more abundant in the Aguilar del Río Alhama Formation.

Fig. 5. Photographs showing the alternation of layers of carbonate mudstone and calcite and quartz pseudomorphs after gypsum of the Oncala Group. (A) Field photograph showing the continuous parallel lamination that characterizes the alternation of layers of carbonate mudstone and pseudomorphs after gypsum. (B) Field photograph of the alternation of laminae of carbonate mudstone and pseudomorphs after lenticular gypsum (arrows). Diameter of the coin is 23 mm. (C) Thin-section photomicrograph of the alternation of laminae of carbonate mudstone (dark colour) and calcite pseudomorphs after gypsum (light colour). Note that the carbonate mudstone laminae contain dispersed pseudomorphs after gypsum (arrows). Plane polarized light. (D) Thin-section photomicrograph of calcite pseudomorphs after gypsum within a carbonate mudstone matrix. Note the euhedral habits of the pseudomorphs. Plane polarized light. (E) Thin-section photomicrograph in plane polarized light of calcite and quartz pseudomorphs after gypsum. Micrite among and within the calcite crystals (white arrows) allows recognition of the lenticular morphology of the original gypsum crystals. Black arrows point to anhydrite inclusions within quartz crystals. (F) Thin-section photomicrograph in cross-polarized light of the calcite and quartz pseudomorphs after gypsum shown in Fig. 5E.

Fig. 6. SEM images of the calcite (Cc) and quartz (Q) crystals that compose the pseudomorphs after gypsum. (A) Calcite and quartz crystals containing anhydrite (A) inclusions. Note the (sub-) idiomorphic shape of some anhydrite inclusions in the quartz. (B) Anhydrite inclusions within quartz. Note the characteristic (sub-) idiomorphic shape of some anhydrite inclusions (arrows). (C) Anhydrite (A) inclusion within calcite. Note that calcite contains also quartz inclusions. (D) Corrosion of quartz by calcite crystals (arrows). Note that quartz contains anhydrite (A) inclusions.

Fig. 7. (A) Typical sequence of the carbonate-evaporitic deposits of the Oncala Group in the eastern area of the Cameros Basin, which shows an increase in the evaporite proportion upwards, and contains carbonate breccias at the top. (B) Photograph of a sample made up of an alternation of laminae of carbonate mudstone (ochre colour) and calcite and quartz pseudomorphs after gypsum (greyish colour) that passes upwards to a carbonate breccia. Note that laminae of calcite and quartz pseudomorphs after gypsum are progressively thicker upwards. Scale bar is in centimetres.

Fig. 8. Field photographs of the carbonate breccias of the Oncala Group, which consist of carbonate mudstone fragments (ochre colour) floating in a calcite and quartz matrix (greyish colour). (A) Chaotic carbonate breccia (yellow arrow) interbedded with unbrecciated layers of alternating carbonate mudstone and calcite and quartz pseudomorphs after gypsum (red arrow). Note that the upper contact of the breccia is irregular. (B) Chaotic carbonate breccias associated with folds. Note that the carbonate breccias occur in the folded area (white arrows), and they pass laterally to an unbrecciated (or very slightly brecciated) alternation of carbonate mudstone and calcite and quartz pseudomorphs after gypsum layers (red arrows). Coin is 2.3 cm in diameter.

(C) Carbonate breccia related with deformation structures. Notice that the most intense brecciation and displacement of the fragments occurs in the core of the fold (arrow). (D) Interstratal chaotic carbonate breccias (white arrows) interbedded with unbrecciated alternating layers of carbonate mudstone and calcite and quartz pseudomorphs after gypsum (red arrows). Coin is 2.3 cm in diameter.

Fig. 9. Schematic diagrams of the carbonate breccias of the Oncala Group, which consist of fragments of carbonate mudstone floating in a matrix made up of calcite and quartz crystals. Breccia fragments and matrix have identical compositions to the associated unbrecciated layers of carbonate mudstone and calcite and quartz pseudomorphs after gypsum, respectively. The fragments in the breccias are from very slightly displaced to chaotically arranged, and their orientation commonly allows recognition of folds. Deformation and brecciation is more intense in thinner carbonate mudstone layers that alternate with comparatively thicker calcite and quartz layers. (A) Carbonate breccia showing irregular upper and lower contacts with unbrecciated layers and polyharmonic folds, formed by brecciation of multi-layered sequences. (B) Carbonate breccia showing sharp lower and upper limits.

Fig. 10. Field photographs of the carbonate breccias of the Oncala Group. (A) Carbonate breccia formed by very slightly displaced carbonate mudstone fragments (ochre colour) floating in a calcite and quartz groundmass (greyish colour). (B) Carbonate breccias showing slightly displaced carbonate mudstone fragments (ochre colour) that allow recognition of centimetre-scale folds. Note that the most intense brecciation occurs in fold cores (arrows). (C) Folded and brecciated alternation of layers of carbonate mudstone (ochre colour) and calcite and quartz pseudomorphs after

gypsum (greyish colour), which show different degrees of brecciation. Thicker carbonate mudstone layers are unbroken (black arrow) or slightly broken (red arrow), whereas thinner carbonate mudstone layers alternating with relatively thicker layers of pseudomorphs after gypsum are intensely brecciated and show a chaotic fabric (white arrow). (D) Carbonate breccia preserving the original stratigraphic bedding and showing intense folding.

Fig. 11. Thin-section photomicrographs of the carbonate breccias. (A) Carbonate mudstone fragments (dark colour) floating in a calcite and quartz matrix (light colour in the left part of the thin section). Right part of the thin section is stained with Alizarin Red S, which causes calcite to show a reddish colour and quartz remains unstained. Note that the original bedding of the carbonate mudstone fragments is preserved, and that thicker carbonate mudstone fragments are slightly rotated, whereas thinner fragments are more intensely displaced. Notice that carbonate mudstone fragments contain disperse calcite and quartz pseudomorphs after gypsum (arrows). Plane polarized light. (B) Carbonate breccias formed by fracturing and rotation of carbonate mudstone laminae, whose original bedding is preserved. Matrix consists of calcite and quartz crystals (light colour in the left part of the thin section). Right part of the thin section is stained with Alizarin Red S, which causes calcite to show a reddish colour and quartz remains unstained. Plane polarized light. (C) Carbonate breccia made up of carbonate mudstone fragments (dark colour) floating in a calcite groundmass (light colour). Note that calcite crystals contain abundant micrite inclusions. Plane polarized light. (D) Photomicrograph in cross-polarized light of the carbonate breccia shown in Fig. 11C. (E) Carbonate breccia formed by fracturing and displacement of carbonate mudstone laminae. Carbonate fragments orientation allows recognition of folds in the

upper part of the photograph. Note that the fragments are more intensely displaced in the folded area than in the unfolded lower part of the photograph. Notice that thin carbonate mudstone laminae are broken into smaller fragments and are more intensely displaced (orange arrows). Matrix consists of a groundmass of cloudy calcite and cloudy quartz (black arrows). Plane polarized light.

Fig. 12. Photographs showing the alternation of dolomudstone and gypsum layers of the lower part of the Oncala Group in the easternmost area of the Cameros Basin (stratigraphic section of Cervera, Figs. 2, 3). (A) Field photograph of the continuous parallel lamination that characterizes the alternation of dolomudstone (dark colour) and gypsum (light colour) layers. Note that gypsum layers are as thick as carbonate layers. (B) Field photograph of a dolomudstone layer with disperse lenticular moulds of gypsum crystals (arrows). (C) Thin section photomicrograph of the alternation of xenotopic granular gypsum laminae (light colour) and fractured dolomudstone laminae (dark colour). Note strong resemblances between this thin section and that of Fig. 11B. Plane polarized light. (D) Photomicrograph in cross-polarized light of the alternation of gypsum laminae and brecciated dolomudstone laminae shown in Fig. 12C. (E) Thin section photomicrograph of macrocrystalline gypsum with inclusions of anhydrite (red arrows). Minor xenotopic, ameboid, cloudy gypsum is also present. Cross-polarized light. (F) Macrocrystalline quartz (Q) with anhydrite inclusions (arrows) in a layer mainly composed of xenotopic, irregular, cloudy gypsum (G).

Fig. 13. (A) Schematic diagram of the polyharmonic folding developed in the lower part of the Oncala Group in the eastern area of the basin (cf. Fig. 13B). The larger-scale folds with amplitudes of tens of metres contain parasitic folds with amplitudes of

decimetres to metres, which in turn include folds with amplitudes of millimetres to centimetres. The upper part of the represented multilayer sequence does not display folds with amplitudes of tens of metres but it shows folds with amplitudes of decimetres to metres containing parasitic folds of millimetres to centimetres. (B) Southwest-Northeast panoramic photograph of large-scale folds with amplitudes of tens of metres (see Fig. 2 for location). The uppermost layers in the photo are apparently undeformed in this view, but they contain folds with amplitudes of decimetres to metres and parasitic folds with amplitudes of millimetres to centimetres (see Fig. 13A for schematic diagram). The yellow lines indicate key beds deformed by folds with amplitudes of tens of metres, the blue lines indicate key beds not affected by folding with amplitudes of tens of metres. A satellite image of this area is shown in Fig. 14, in which the same key beds and letters (a,b,c) are marked to make easier the comparison of both figures. The arrow points to the stratigraphic level that corresponds laterally to the one marked in Fig. 4A.

Fig. 14. Satellite image of intensely deformed deposits of the Aguilar del Río Alhama Formation that show folds with amplitudes of tens of metres trending approximately NW-SE. These structures are aligned with a major, NW-SE trending, syncline in the region (see Fig. 2 for location). Note that the deformation is more intense in the lower layers (yellow lines), while the overlying layers (dashed blue lines) do not show large-scale deformation. A panoramic photograph of this area is shown in Fig. 13B. Letters a, b and c are located in the same places than those of Fig. 13B to allow comparison.

Fig. 15. Field photographs of deformation structures affecting (A-D) the alternation of layers of carbonate mudstone (ochre colour) and calcite and quartz pseudomorphs after

gypsum (grey colour), and (E-G) the alternation of layers of dolomudstone (dark colour) and gypsum (light colour) of the lower part of the Oncala Group in the easternmost area of the Cameros Basin (stratigraphic section of Cervera, Figs. 2, 3). (A) Folds with amplitudes of decimetres in the stratigraphic level indicated with an arrow in Figs. 4A and 13B. (B) Folds with amplitudes of centimetres in the stratigraphic level indicated with an arrow in Figs. 4A and 13B. (C) Polyharmonic folds causing brecciation and slight displacement of the carbonate mudstone layers. Coin is 23 mm in diameter. (D) Detail of centimetre-scale folds shown in Fig. 15C. Note the brecciation of the carbonate mudstone layers. Coin is 23 mm in diameter. (E) Intensely deformed multi-layered sequence of alternating dolostone and gypsum. Hammer for scale in the lower part of the photograph. (F) Field photograph of alternating layers of dolostone and gypsum deformed by folds with amplitudes of few centimetres. Folded dolostone layers are fragmented into centimetre-size rectangular prisms. (G) Interstratal overturned folds deforming few layers of dolostone and gypsum (arrow). Note that the underlying and overlying strata are undeformed.

Fig. 16. Characteristic features of tectonic sulphate-flow breccias (based on the breccias of the Oncala Group studied in this work) and comparison with evaporite-solution collapse breccias (based mainly on Warren, 2006; Flügel, 2010) and slump breccias (based mainly on Woodcock, 1976; Martinsen, 1994; Flügel, 2010), which share some features with the studied breccias.

Table 1. Attitude of the axial planes of the decimetre to metre-scale folds within the deposits of the Oncala Group.

Table 2. Measurements of the bedding within the Pégado anticline, and calculated attitude of the axial plane of the fold.

Table 3. Measurements of the bedding within the Inestrillas syncline, and calculated attitude of the axial plane of the fold.

UTM coordinates of the measurement sites (ETRS 1989)	Strike	Dip
580897, 4639987	N172ºE	32ºW
580791, 4640386	N180ºE	30ºW
580966, 4641452	N6ºE	34ºW
580944, 4642026	N170ºE	42ºW
	N160ºE	32ºSW
580880, 4642803	N160ºE	22ºSW
	N154ºE	20ºSW
580307, 4643510	N2ºE	24ºW
580415, 4644120	N4ºE	32ºW
580665, 4644549	N70ºE	36ºNW
580580, 4644805	N66ºE	30ºNW
580892, 4645120	N72ºE	32ºNW
581420, 4645394	N102ºE	42ºN
581746, 4645569	N106ºE	26ºN
581759, 4645649	N100ºE	40ºN
582116, 4645959	N92ºE	46ºN
582116, 4646020	N104ºE	42ºN
582376, 4646108	N100ºE	44ºN
582734, 4646311	N109ºE	44ºNE
583495, 4645842	N110ºE	55ºNE
584181, 4645639	N118ºE	38ºNE
584192, 4645283	N120ºE	50ºNE
	N132ºE	40ºNE
585638, 4644781	N134ºE	18ºNE
585722, 4644334	N142ºE	42ºNE
586089, 4642794	N136ºE	48ºNE
583807, 4642606	N156ºE	55ºNE
Calculated attitude of the Pégado anticline	N146ºE	72ºNE

UTM coordinates of the measurement sites (ETRS 1989)	Strike	Dip
585638, 4644781	N134ºE	18ºNE
585722, 4644334	N142ºE	42ºNE
586089, 4642794	N136ºE	48ºNE
586087, 4642606	N156ºE	55ºNE
586475, 4644645	N30ºE	25ºNW
586563, 4644744	N6ºE	52ºW
	N170ºE	58ºW
	N160ºE	40ºSW
585614, 4646259	N160ºE	32ºSW
586001, 4646252	N172ºE	36ºW
586084, 4645986	N156ºE	44ºSW
Calculated attitude of the Inestrillas syncline	N155ºE	80ºNE

UTM coordinates of the measurement site (ETRS 1989)	Strike	Dip
580406, 4647540	N130ºE	24ºSW
	N128ºE	72ºSW
	N122ºE	60ºSW
	N130ºE	16ºSW
	N146ºE	22ºSW
	N138ºE	70ºNE
	N144ºE	16ºSW
	N120ºE	24ºSW
	N128ºE	18ºSW
	N114ºE	26ºSW
	N140ºE	58ºNE
580423, 4647611	N150ºE	86ºSW
	N156ºE	70ºSW
	N188ºE	34ºW
	N168ºE	70ºSW
	N140ºE	30ºSW
	N158ºE	74ºSW
	N148ºE	54ºSW
	N142ºE	48ºSW
	N147ºE	50ºSW
	N140ºE	50ºSW
	N157ºE	40ºSW
	N164ºE	58ºSW
	N142ºE	67ºSW
	N155ºE	65ºSW
	N136ºE	86ºSW
	N160ºE	52ºSW
	N132ºE	72ºSW
580774, 4647698	N136ºE	90º
	N146ºE	60ºSW
	N138ºE	72ºSW
	N153ºE	80ºSW
	N143ºE	74ºSW
	N112ºE	85ºSW
	N110ºE	86ºSW
	N145ºE	90º
	N100ºE	46ºN
	N107ºE	90º
	N132ºE	80ºSW
	N124ºE	90º
	N172ºE	84ºW
	N136ºE	50ºSW
	N138ºE	78ºSW
	N161ºE	82ºSW
	N154ºE	78ºSW
	N130ºE	52ºSW
	N144ºE	76ºSW
	N136ºE	68ºSW
	N142ºE	72ºSW
	N144ºE	84ºSW
	N138ºE	88ºSW

	N148ºE	70ºSW
	N146ºE	80ºSW
	N100ºE	92ºW
	N150ºE	80ºSW
	N180ºE	48ºW
	N150ºE	80ºSW
	N108ºE	90º
	N128ºE	88ºSW
	N134ºE	88ºSW
	N140ºE	68ºSW
	N128ºE	78ºSW
	N142ºE	60ºSW
	N118ºE	48ºSW
	N132ºE	56ºSW
	N134ºE	68ºSW
584681, 4651464	N6ºE	78ºW
	N160ºE	60ºNE
	N172ºE	90º
	N176ºE	24ºW
	N164ºE	80ºNE
	N40ºE	82ºNW
	N176ºE	66ºE
	N24ºE	84ºNE
	N165ºE	52ºNE
	N170ºE	82ºE
	N140ºE	66ºNE
585167, 4647883	N120ºE	70ºSW
	N118ºE	60ºNE
	N172ºE	66ºW
	N113ºE	80ºSW
	N130ºE	70ºNE
	N131ºE	46ºNE
	N140ºE	88ºNE
	N128ºE	82ºNE
	N149ºE	80ºNE
	N136ºE	64ºSW
585722, 4644334	N128ºE	50ºSW
	N128ºE	50ºSW
	N136ºE	64ºSW
	N138ºE	70ºSW
	N138ºE	70ºSW
	N138ºE	70ºSW
	N126ºE	82ºSW
	N140ºE	65ºSW
	N98ºE	74ºN
	N128ºE	68ºSW
	N152ºE	58ºSW
	N138ºE	78ºSW